

COMPUTATIONAL STUDY ON THE Cu-RICH SIDE OF ALUMINUM-COPPER PHASE
DIAGRAM

by

Khaled Ahmed Hirmas

Presented to the Faculty of the Graduate School of
The University of Texas at Arlington in partial fulfilment of the requirement
for the degree of

DOCTOR OF PHILOSOPHY

THE UNIVERSITY OF TEXAS AT ARLINGTON

August 2018

To my Family

ACKNOWLEDGEMENTS

I would like to express my great appreciation and thanks to Prof. Choong-Un Kim, who gave me an opportunity to do my research in his group, also for his guidance, suggestions and encouragement not only during my research work but also during my study. I also would like to thank all my committee members, Dr. Hao, Dr. Koh, Dr. Michael and Dr. Cao for their time.

I would also like to express my gratefulness to the department secretaries, Jennifer Standlee, Beth Robinson, and Natalie Burden for his for their support.

The warmest thanks from the bottom of my heart go to my family for ...

Arlington, July 29, 2018

ABSTRACT

Computational study on the Cu-rich side of Al-Cu Phase Diagram

Khaled Hirmas

The University of Texas at Arlington, 2018

Supervising professor: Choong-Un Kim

Cu-rich side of Al-Cu phase diagram has not been studied extensively as the Al-rich side. It is well established that a one-phase (α phase) exists at 300°C between the 82% Cu and pure Cu, and at the eutectic temperature (1032°C) between 86% Cu and pure Cu, α phase, when quenched from above 600°C and subjected to annealing below about 300°C, or deformation, show ordering effects in resistivity, heat capacity, diffuse X-ray, microstructure, and in mechanical properties. This has been studied to determine whether these effects are due to short-range or long-range ordered domain [1]. The present computational study is to assess the Cu-rich side of Al-Cu phase diagram for Cu concentration larger than 75%, and between 300K and 1000K. Molecular dynamics, Hybrid Molecular Dynamics/Monte Carlo, and DFT simulations are used to investigate the possibility of phase separation in this range of phase diagram. It is shown that a two-phase region exists below about 900K, and that phase separation takes place by nucleation and growth, and not by spinodal decomposition. Also, it is shown that these two phases are random FCC α solid solution, and intermetallic α_2 .

TABLE OF CONTENTS

Acknowledgements.....	ii
Abstract.....	iii
List of figures.....	vii
List of tables.....	x
Introduction.....	1
Chapter 1: Simulation Methods Principles.....	3
1.1 Molecular Dynamics.....	3
1.1.1 Interatomic potentials.....	6
1.1.1.1 Embedded atom method (EAM)	6
1.2 Calculation of thermodynamic variables.....	9
1.2.1 Temperature and instantaneous temperature.....	10
1.2.2 Temperature control.....	11
1.2.3 Pressure and instantaneous pressure.....	12
1.2.4 Pressure control.....	13
1.3 Hybrid MD/MC simulation.....	14
1.3.1 Canonical ensemble (constant N, V, T).....	14
1.3.2 Semi-grand canonical ensemble (constant N, V, T, $\Delta\mu$).....	16
1.3.3 Variance-constrained semi-grand canonical ensemble.....	17
1.4 Density Functional Theory.....	18

1.4.1 The Hohenberg-Kohn theorems.....	20
1.4.2 Kohn-Sham equations.....	24
1.4.3 The pseudopotential.....	26
1.4.4 Electrons in solids.....	27
Chapter 2: Molecular Dynamics and Hybrid MD/MC Computations.....	30
2.1 Computational procedure.....	30
2.2 Results and discussions.....	32
2.2.1 Convergence test.....	38
2.2.2 Visualization results.....	39
2.2.3 Modification of the Cu-rich side of Al-Cu phase diagram.....	43
Chapter 3: DFT Computations.....	45
3.1 Computational procedure.....	45
3.2 Results and discussion.....	45
3.2.1 Aluminum Bulk properties.....	45
3.2.2 Copper Bulk properties.....	48
3.2.3 Energetics of intermetallics and Al-Cu alloys.....	51
3.2.3.1 The energetics of $L1_2$ ($AlCu_3$).....	51
3.2.3.2 The energetics of $D0_{22}$ ($AlCu_3$).....	52

3.2.3.3 Energetics of Al-Cu solid solutions.....	54
Summary.....	56
Appendix A: LAMMPS CODES (MOLECULAR DYNAMICS) used in this work.....	59
Appendix B: QUANTUM ESPRESSO CODES (DFT) used in this work.....	71
References.....	77
Biographical information.....	84

LIST OF FIGURES

Figure 1.1 Electron density for water molecule.....	21
Figure 1.2 The construction of pseudopotential.....	26
Figure 1.3 The irreducible Brillouin zone (IBZ).....	28
Figure 2.1 Schematic representation of the simulation procedure for the smaller supercells.....	32
Figure 2.2. Chemical potential difference as a function of concentration for smaller supercell Cu starting state at 300K.....	33
Figure 2.3 Chemical potential difference as a function of concentration for smaller supercell Al starting state at 300K.....	34
Figure 2.4 Chemical potential difference as a function of concentration for smaller supercell Al ₄ Cu ₉ starting state at 300K.	34
Figure 2.5 Chemical potential difference as a function of concentration for smaller supercell Cu starting state at 700K.....	35
Figure 2.6 Chemical potential difference as a function of concentration for smaller supercell Al ₄ Cu ₉ starting state 1000K.	35
Figure 2.7 Chemical potential difference as a function of concentration for smaller supercell Cu starting state 800K.	36
Figure 2.8 Chemical potential difference as a function of concentration for larger supercell Cu starting state at T=300K.	36

Figure 2.9 Chemical potential difference as a function of concentration for larger supercell Cu starting state at T=700K.	37
Figure 2.10 Chemical potential difference as a function of concentration for larger supercell Cu starting state at T=1000K.	37
Figure 2.11 Enthalpy of mixing at 300K for smaller supercell Cu starting state.....	38
Figure 2.12 Convergence test at 300 K.....	39
Figure 2.13 Atomic configurations (a) just after alloying the sample (α phase), (b) after the initial 5E5 steps (1000MC steps), (c) after the additional 1E5 steps (1000MC steps)	40
Figure 2.14 The four monoatomic slices cut along [001] direction which show clearly the L1 ₂ and D0 ₂₂ structures outlined by a square and a rectangle respectively.....	41
Figure 2.15 L1 ₂ and D0 ₂₂ crystal structures.....	41
Figure 2.16 The four monoatomic slices cut along [001] direction which show clearly the L1 ₂ and D0 ₂₂ structures respectively.....	42
Figure 2.17 The two-phase region is constructed from the extremities of concentration jump at 300, 700, 800K.....	43
Figure 2.18 Modification of the Cu-rich side of Al-Cu phase diagram.....	44
Figure 3.2 Convergence test for bulk Aluminum with respect to unshifted and shifted k-points grids.....	46
Figure 3.3 Convergence test for bulk Aluminum with respect to energy cutoff.....	46

Figure 3.4 Convergence test for isolated Aluminum atom with respect to energy cutoff.....	47
Figure3. 5 The plot of cohesive energy versus series of lattice parameters or unit cell volumes for Aluminum.....	48
Figure 3.6 Convergence tests for bulk Copper with respect to shifted and unshifted k-points grids.....	49
Figure 3.7 Convergence test for bulk Copper with respect to energy cutoff.....	49
Figure 3.8 Convergence test for isolated Copper atom with respect to energy cutoff.....	50
Figure 3.8 The plot of cohesive energy versus series of unit cell volumes for Copper.....	50
Figure 3. 9 The plot of total energy versus series of unit cell volumes for Copper.....	52
Figure 3.10 The heat map of c/a versus a for D0 ₂₂ AlCu ₃ structure.....	53
Figure 3.11 The two supercells used in the calculations of mixing enthalpy of 6.25% Al and 12.5% Al solid solutions	55

LIST OF TABLES

Table 2.1 Comparison of four different interatomic potentials in terms of formation energy...30

INTRODUCTION

It is well established that the solubility limit of Al in Cu is about 19.7% at eutectoid temperature (567 °C) and it does not change down to peritectoid temperature (363 °C). Below 363 °C, the solubility decreases and reaches to less than 17% Al. The α_2 phase which is in equilibrium with γ_1 and α at 363 °C was discovered by West and Thomas [1]. TTT [2] and structural studies [1, 3-6] were carried out on the structure and the composition of α_2 phase and it was found that it has an ordered FCC structure based on $L1_2$ and $D0_{22}$ with long-period superlattice. α phase exists below the eutectic temperature (1032°C) between 86% Cu and pure Cu, and between 82% Cu and pure Cu at 300°C. When α phase is quenched from above 600°C and subjected to annealing below about 300°C, or deformation, show ordering effects in resistivity, heat capacity, diffuse X-ray, microstructure, and in mechanical properties. This has been studied to determine whether these effects are due to short-range or long-range ordered domain. To attain order in this range of composition and temperatures the annealing process should be carried out for enough time. This time varies from one researcher to another, and this could explain the controversy of whether the obtained structures have long or short order domains. Shorter annealing times could lead to the entrapment in a metastable configuration, hence short-order structures, and vice versa. This controversy is addressed here using three simulation methods, namely Molecular Dynamics (MD), Hybrid (Monte Carlo)MC/MD, and Density Functional Theory (DFT). Molecular Dynamics is basically used to select the proper interatomic potential that will be used in Hybrid MC/MD simulations. Hybrid MC/MD simulations in either the canonical (C) or semi-grand canonical (SGC) ensembles are used to study phase separation in this system. In hybrid MD/MC simulation, transmutation Monte Carlo simulations is alternated with molecular dynamics steps. This leads to faster equilibration, hence resolves the above-mentioned controversy. It also leads to better

chemical mixing and precipitation as well as thermal vibrations. DFT simulation is used to confirm the results obtained from MD and Hybrid MC/MD. The theoretical aspects of these three simulation methods are discussed in the first chapter. The results obtained MD Hybrid MC/MD simulations are presented and discussed in the second chapter, while the third chapter is devoted to the results and discussion of the DFT simulations.

Chapter 1: Simulation Methods Principles

1.1 Molecular Dynamics:

Molecular dynamics (MD) is a simulation technique that is used to study the dynamics of a given set of atoms or molecules as classical particles within the framework of classical mechanics. Their equations of motion are described by the second Newton's law of motion. The force exerted by neighbor particles on particle i whose position is defined by the position vector \mathbf{r}_i is given by

$$\mathbf{F}_i(\mathbf{r}_i) = m_i \frac{d^2 \mathbf{r}_i}{dt^2} \quad i = 1, 2, \dots, N \quad (1)$$

Different types of interatomic potentials, $U(\mathbf{r}_i)$, that represent the potential energy of a given arrangement of particles, are used to define the interactions between the particles. The gradient of this potential determines the

$$\mathbf{F}_i = -\nabla U(\mathbf{r}_i) \quad (2)$$

The interatomic potential is given in its simplest form by a sum of pairwise interactions

$$U = \frac{1}{2} \sum_{i=1}^N \sum_{j \neq i}^N u(r_{ij})$$

where $r_{ij} = |\mathbf{r}_i - \mathbf{r}_j|$. Therefore, the force on atom i is given by the sum of the forces exerted by all other j atoms

$$\mathbf{F}_i = \sum_{j \neq i}^N \mathbf{f}_{ij}, \quad \text{where } \mathbf{f}_{ij} = \left(-\frac{du(r_{ij})}{dr_{ij}} \right) \left(\frac{\mathbf{r}_{ij}}{r_{ij}} \right) \quad (4)$$

From the initial conditions, $\mathbf{r}_i(t_0)$ and $\mathbf{v}_i(t_0)$, at time $t = t_0$ and the interatomic potential, the equations of motion are solved numerically using different algorithms. For example, using

the Velocity Verlet [7] algorithm, the positions and velocities after a short timestep Δt , usually less than few femtoseconds, are computed as follows:

$$\mathbf{r}(t + \Delta t) = \mathbf{r}(t) + \mathbf{v}(t)\Delta t + \frac{1}{2}\mathbf{a}(t)\Delta t^2 \quad (5)$$

$$\mathbf{v}(t + \Delta t) = \mathbf{v}(t) + \frac{1}{2}\{\mathbf{a}(t) + \mathbf{a}(t + \Delta t)\}\Delta t \quad (6)$$

During this timestep Δt , the forces are assumed to be constant and the state of the system after it, is defined by atomic positions $\mathbf{r}(t + \Delta t)$. At the end of simulation time, which is typically few nanoseconds [8], the trajectories of atoms in the system are obtained.

Beside it is being in principle deterministic in terms of positions and velocities, molecular dynamics also generates many configurations (microscopic states) whose distribution in different ensembles is governed by statistical mechanics using different statistical distribution functions. A system in certain macrostate, defined for example by thermodynamic quantities such as the number of atoms (N), pressure (P), temperature(T) has different microstates (configurations) and is called ensemble; in this case it is the *Isobaric Isothermal Ensemble*. The probability with which a given microstate at a given moment of time is described by the microscopic probability distribution function in this ensemble.

Obtaining the trajectories is not always the case. Thermodynamic properties can be obtained from molecular dynamics information by averaging with respect to time (over the microstates) and all atoms according to statistical mechanics.

Molecular dynamics is not only used to study small structures like small clusters of atoms or nanomaterials, but also can be used to study bulk materials by imposing proper boundary conditions on the simulation box [9]. A common choice is the three-dimensional periodic boundary

conditions which introduce identical images of the system (supercell), hence filling the space around the simulation box. This keeps the number of particles in the simulation box conserved, for when a particle leaves/enters the simulation box an image particle enters/leaves the simulation box. Using periodic boundary conditions implies that particles are enclosed, hence avoids the occurrence of surfaces. The use of the periodic boundary conditions makes each particle in the simulation box appear to interact with all the particles including the image particles. This is overcome by using interatomic potential with finite range (cut off distance, r_{cut}), beyond which it becomes negligible, and making the simulation box larger than $2r_{cut}$ along each direction.

MD simulations are mainly determined by the time step Δt , the thermostat damping parameter, τ , the barostat damping parameter, τ_p , and the relaxation time, τ_{relax} , which must not exceed system-dependent maximum values. Δt is to be chosen so that fast movements cause only small numerical errors, for which, depending on the type of numerical integrator, at an order of magnitude smaller than the fastest time scale in the system. For example, a timestep of $1fs$ is suitable for solids. τ and τ_p should be chosen large enough to make only minor changes between times, otherwise the dynamics of the system will be disturbed. Typical values are $\tau = 100 \Delta t$ and $\tau_p = 1000 \Delta t$. Finally, the relaxation time τ_{relax} must be larger than the oscillations of the temperature and the pressure produced by the thermostat and Barostat. τ_{relax} is usually defined as the largest time scale for molecular or atomic motion. Diffusion times are usually used to estimate the relaxation time in solids. For equilibration to take place, equilibration time should exceed τ_{relax} by several times.

1.1.1 Interatomic potentials:

The interatomic potential is the most important feature in molecular dynamics simulation. It describes the potential energy of the system as a function of its coordinates; therefore, it should have two important features; the repulsion interaction at small interatomic distances, and the attraction interaction that is responsible for the keeping the atoms from being torn apart [8]. The need to describe the interatomic interactions in different materials lead to the development of several formalisms of interatomic potentials [8]. Lennard-Jones potential, the most prominent example of pair potential [10], has been used in the simulations of many different problems, for it is computationally simple. But applying this pair potential does not describe the environmental dependence because it treats the atoms in the bulk in the same way as the atoms on the surface or near a defect [11]. Moreover, Transition metals which have partially filled *d* subshells that contribute to bonding with partial covalent bond cannot be described by the pair potential because of the directional nature of the covalent bond. To describe interaction in metals and alloys, alternative potentials developed in different formalisms such as embedded atom method (EAM) [6], modified embedded atom method [7], and the Finnis-Sinclair (FS)scheme [8].

1.1.1.1 Embedded atom method (EAM):

The need to overcome the draw backs of pair potentials and for better simulation studies lead to the development of an alternative to it by Daw and Baskes [10,15]. This potential is based on density-functional ideas which they call the embedded-atom method (EAM) [10,12,15]. EAM has been used successfully to study many problems. Examples of these studies include segregation and phase separation in alloys [16-20], point defects, dislocations, plastic deformation, and fracture properties [10,15,21-25]. Daw and Baskes made use of density-functional theory which states that the total electronic energy for an arbitrary arrangement of N atoms can be written as a unique

functional of the total electron density [11] and the electron density in a metal can be approximated by the linear superposition of atomic electron densities. They approximated the total energy of N atoms as the sum of the energies required to embed each atom individually within the homogeneous electron density due to the other atoms plus the electrostatic energy, pair-potential, due to core-core overlap. The total energy, U_{tot} , is expressed as

$$U_{tot} = \sum_i F_i(\rho_i) + \frac{1}{2} \sum_i \sum_{j \neq i} \varphi_{ij}(r_{ij}) \quad (7)$$

Here, ρ_i is the superposition of atomic electron densities, f_j , at atom i due to all other atoms, j , of the system,

$$\rho_i = \sum_{j \neq i} f_j(r_{ij}) \quad (8)$$

$F_i(\rho_i)$ represents the energy required to embed atom i in the electron density ρ_i , $\varphi_{ij}(r_{ij})$ is the pair-potential between atoms i and j , and r_{ij} is the distance between atom pairs, i and j . $F_i(\rho_i)$, and $\varphi_{ij}(r_{ij})$ depends on the underlying physical system and their approximate expressions are obtained within the framework of density-functional theory. The accurate description of these functions is determined by fitting the EAM potential to known bulk properties, such as sublimation energy, lattice constant, elastic constants, vacancy formation energy. The choice of physical properties used to calibrate the potential may have a significant effect on the applicability of the potential for simulation, and care should be given in selecting a potential for simulation and interpreting results [26]. For example, Banerjee and Smith proved that a simple exponential function that represents the atomic electron density in the bulk, near-vacancies, and free surfaces is given by [27].

$$f(r) = f_e \cdot \exp[-\chi(r - r_e)] \quad (9)$$

f_e is a scaling constant that is eliminated upon substitution of **Equation (9)** in **Equation (10)** and r_e is the equilibrium interatomic spacing. Also, they developed embedding energy function that has the following form

$$F(\rho) = -F_o \left[1 - \ln \left(\frac{\rho}{\rho_e} \right)^n \right] \left(\frac{\rho}{\rho_e} \right)^n + F_1 \left(\frac{\rho}{\rho_e} \right) \quad (10)$$

where $F_o = E_c - E_v$, E_c is the cohesive energy, and E_v is the vacancy formation energy $n = 0.5$ and ρ_e is the equilibrium electron density. An example of the pair potential that can be cited here is the one developed by Rose *et al.* [22].

$$\varphi(r) = -\alpha[1 + \beta(r/r_a - 1)]\exp[-\beta(r/r_a - 1)] \quad (11)$$

$\chi, F_1, \alpha, \beta, r_a$ and χ are adjustable parameters that must be determined in fitting process.

The embedding function does not depend on the source of background electron density, hence can still be used in developing EAM potential for the alloys. Johnson in his model [22] used an electronic density weighted combination of the atomic pair potentials to describe the cross pair-potential of an alloy composed of atomic species a and b

$$\varphi^{ab}(r) = \frac{1}{2} \left[\frac{f^b}{f^a} \varphi^{aa}(r) + \frac{f^a}{f^b} \varphi^{bb}(r) \right] \quad (12)$$

For the alloy system, the scaling factor f_e in **Equation (9)** for an alloy system is no longer arbitrary and it is given such that it contains adjustable parameter that is used to fit the EAM alloy potential to the dilute-limit heat of solution of the alloy. An example for that is

$$f_e = (\Omega/E_c)^\delta \quad (13)$$

where Ω is the atomic volume, E_c is the cohesive energy of the element, and δ is the adjustable parameter.

1.2 Calculation of thermodynamic variables:

For the calculation of thermodynamic state variables in MD simulations such as temperature and pressure of a particle system, the computed average is used. This can be calculated as follows (see [29]):

Given the values of a physical observable as A_1, A_2, \dots, A_i , the computed average of A for a period equal to the production period is given by

$$\langle A \rangle = \frac{1}{N} \sum_{i=0}^N A_i \quad (1)$$

The time average of A for infinite time is given by

$$\langle A \rangle_t = \lim_{\tau \rightarrow \infty} \frac{1}{\tau} \int_0^{\tau} A(t) dt \quad (2)$$

In MD simulations and according to ergodic hypothesis, these two averages are equivalent for a suitable choice of time step size Δt and a sufficient number of measuring points [400]. In ergodic systems, therefore, the approximate calculation of the ensemble averages of an observable (that is, the computation of a thermodynamic state variable of a Systems) by means of a computed average is possible and permissible [30]. If the system is in thermodynamic equilibrium, the computed thermodynamic state variables such temperature or pressure, show no more drift but they fluctuate around the average value. Conversely, if these quantities are drifting, this means that the system did not reach equilibrium [30, 31].

1.2.1 Temperature and instantaneous temperature:

In MD simulations, it makes sense to look at the instantaneous temperature. Because of this the temperature T of the system can be calculated. The instantaneous temperature $T_{inst}(t)$ to the time t is defined as follows:

$$T_{inst}(t) = \frac{2E_{kin}(t)}{\mathcal{F}k_B} = \frac{1}{\mathcal{F}k_B} \sum_{i=1}^M m_i |\mathbf{v}_i(t)|^2 \quad (3)$$

where E_{kin} is the kinetic energy, \mathcal{F} is the number of degrees of freedom, and m_i is the mass of the particle

If the total momentum of the system is zero, then from the equipartition theorem of thermodynamics [32],

$$T = \frac{2\langle E_{kin} \rangle}{\mathcal{F}k_B} = \langle T_{inst} \rangle \quad (4)$$

The temperature T is thus given by the average value of the instantaneous temperature. If the momentum of the total system is not zero, the particles velocities are determined by subtracting the center-of-mass velocity before applying **equation (4)**. As can be seen from **equation (4)**, the number of degrees of freedom \mathcal{F} of the particle system must be known to calculate the temperature. In atomic systems, the number of degrees of freedom is $3N$ (one degree of freedom in each direction). When using periodic boundary conditions, this number is reduced to $3N - 3$, since the translation of the entire system is ignored [31].

As an example, in N -particles system closed system, where the number of particles N and the total energy E of the system are constant, and there is no energy or material exchange (NVE ensemble in statistical physics), the system temperature adjusts itself over time.

In molecular dynamics, velocity rescaling is a very simple process in which a desired target temperature can be set in a particle system. This can be achieved by rescaling the particles velocities, which is carried out at regular time intervals (approximately every 10 to 50 integration steps) by

$$v_{new} = \lambda v_{old} \quad (5)$$

where, v_{new} , v_{old} are the new and old velocities, and λ is the scaling factor which is given by

$$\lambda = \sqrt{\frac{T}{T_{inst}}} \quad (6)$$

It should be noted that due to the regular scaling natural fluctuations of the particles velocities are suppressed. Because of this, this procedure cannot be used to create realistic thermodynamic ensemble [31], therefore, different thermostats are devised to control the temperature.

1.2.2 Temperature control:

As already mentioned, the particle system can be brought to a desired temperature T by means of velocity rescaling, although no realistic thermodynamic ensemble can be produced in this procedure. Another way to control the temperature is to couple the system to a heat reservoir.

This coupling can be achieved by introducing a friction term, $\zeta(t)m_i\mathbf{v}_i(t)$, in Newton's equations of motion [33]. The equation of motion then becomes

$$m_i\mathbf{a}_i(t) = \mathbf{F}_i(t) - \zeta(t)m_i\mathbf{v}_i(t), i = 1, \dots, N \quad (7)$$

where $\zeta(t)$ is a function to be specified

The system becomes energy deprived when $\zeta(t)$ is positive and energy is supplied when $\zeta(t)$ is negative. How fast the energy exchange takes place depends on the choice for $\zeta(t)$. Various

proposals can be found in [31, 33]. For the so-called Nosé-Hoover thermostat (NVT-ensemble) [34, 35] the following differential equation is used for

$$\frac{Q}{2} \frac{\partial \zeta(t)}{\partial t} = \frac{1}{2} \sum_{i=1}^N m_i |\mathbf{v}_i(t)|^2 - \frac{1}{2} (\mathcal{F} + 1) k_B T \quad (8)$$

The first term is the actual kinetic energy, and the second term is the desired kinetic energy. The parameter Q is called the thermostat mass and determines the strength the coupling to the heat reservoir. The greater Q is, the weaker is the coupling. From **equation (8)** the control mechanism can also be seen. The slope $\frac{\partial \zeta(t)}{\partial t}$ is positive if and only if the actual kinetic energy is greater than the desired kinetic energy (the system is too hot). As a result, $\zeta(t)$ increases with time, which is due to **equation (7)** ultimately leads to depriving the system of energy (the system gets cooled). In [35] it is shown that configurations in the canonical (NVT) ensemble with temperature T are generated by means of the Nosé-Hoover thermostat. Applying the equations of motion **equation (7)**, **equation (8)** makes the total energy

$$H = \frac{1}{2} \sum_{i=1}^N m_i |\mathbf{v}_i(t)|^2 + U(\mathbf{r}^N) + \frac{\zeta^2 Q}{2} + (\mathcal{F} + 1) k_B T \ln s \quad (9)$$

where s is the position of the heat reservoir, and $\zeta = \dot{s}/s$

1.2.3 Pressure and instantaneous pressure:

In addition to the temperature in MD simulations, the internal pressure, P , of the particle system is calculated. Without using periodic boundary conditions, the pressure, P , is given by virial theorem

$$P = \frac{Nk_B T}{V} + \left\langle \frac{1}{3V} \sum_{i=1}^N \mathbf{r}_i \cdot \mathbf{F}_i \right\rangle \quad (10)$$

For a cubic simulation box with edge L , and with using periodic boundary conditions, the pressure, P , is given [36],

$$P = \frac{Nk_B T}{V} + \left\langle \frac{1}{3V} \sum_{i=1}^N \mathbf{r}_i \cdot \mathbf{F}_i - \frac{1}{3L^2} \frac{\partial U}{\partial L} \right\rangle \quad (11)$$

where $V = L^3$, U is the potential energy.

Like the definition of the instantaneous Temperature T_{inst} , instantaneous pressure P_{inst} at time t can be defined as

$$P_{inst}(t) = \frac{Nk_B T_{inst}}{V} + \left\langle \frac{1}{3V} \sum_{i=1}^N \mathbf{r}_i(t) \cdot \mathbf{F}_i(t) - \frac{1}{3L^2} \frac{\partial U(\mathbf{r}^N(t))}{\partial L} \right\rangle \quad (12)$$

1.2.4 Pressure control:

Andersen developed a method for MD simulations at constant pressure (NPE-ensemble) [37].

This works in a similar way to the temperature control method presented by Nosé and Hoover.

The equations of motion in this case are

$$m_i \mathbf{a}_i(t) = \mathbf{F}_i(t) - \frac{1}{3} m_i \mathbf{r}_i(t) \left(\frac{\ddot{V}}{V} - \frac{2}{3} \left(\frac{\dot{V}}{V} \right)^2 \right), i = 1, \dots, N \quad (13)$$

$$\Upsilon \ddot{V} = \frac{1}{3V} \sum_{i=1}^N m_i \left| \mathbf{v}_i(t) - \frac{1}{3V} \dot{V} \mathbf{r}_i(t) \right|^2 + \frac{1}{3V} \sum_{i=1}^N \mathbf{F}_i(t) \cdot \mathbf{r}_i(t) - P \quad (14)$$

As can be seen from **equation (14)**, the Newton equations of motion come again with a friction term, which is now coupled to the volume V of the simulation box. The parameter $\Upsilon > 0$ determines the lag of the pressure control. Here, the total energy is given by

$$H = \frac{1}{2} \sum_{i=1}^N m_i \left| \mathbf{v}_i(t) - \frac{1}{3} \frac{\dot{V}}{V} \mathbf{r}_i(t) \right|^2 + U(\mathbf{r}^N) + \frac{\dot{V}^2 \Upsilon}{2} + PV \quad (15)$$

In the Andersen method, the size of the simulation box varies with time and the particle number N is constant, which makes the density of the particle system fluctuate. It is possible to combine the Andersen with the Nosé-Hoover method [34, 39]. This allows simulations to be performed at constant pressure and constant temperature (NPT ensemble). The method of Parrinello and Rahman is an extension of the Andersen method [40, 41], as it also allows deformation of the simulation box. Therefore, structural phase transitions can also be simulated with this method. To determine lattice constants in crystalline solids, Andersen method remains the best.

1.3 Hybrid MD/MC simulation:

MC simulations in either the canonical (C) or semi-grand canonical (SGC) ensembles are commonly used to study phase separation in metallic alloys. Variance-constrained semi-grand canonical (VC-SGC) which is an extension of SGC ensembles and combines the advantages of C and SGC ensembles is used to study phase separation too. VC-SGC is a hybrid MD/MC simulation, where transmutation Monte Carlo simulations is alternated with molecular dynamics steps, hence obtaining a powerful tool that considers speedy equilibration, chemical mixing and precipitation as well as thermal vibrations.

1.3.1 Canonical ensemble (constant N , V , T):

Here, the system of constant volume consists of constant number of atoms of each type and is in contact with a very large heat reservoir that allows exchange of energy. The total energy of the

system fluctuates, but the temperature does not. The partition function of this ensemble is given by

$$\mathbb{Z}_C(N, V, T) = \frac{1}{h^{3N} N!} \int e^{-\beta H(\mathbf{p}^N, \mathbf{r}^N)} d\mathbf{p}^N d\mathbf{r}^N \quad (14)$$

where H is the Hamiltonian($H=U+K$), $\beta = \frac{1}{kT}$, N is the number of atoms, h is Plank's constant, $\mathbf{p}^N, \mathbf{r}^N$ are the momentum and position vectors of N atoms. In Monte Carlo simulation, the configurational part of partition function is used

$$\mathbb{Q}_C(N, V, T) = \int e^{-\beta U(\mathbf{r}^N, \boldsymbol{\sigma}^N)} d\mathbf{r}^N \quad (15)$$

where $\boldsymbol{\sigma}^N$ is a spin vector, (1,0) for binary system, that describes the transmutations, hence the dependence of potential energy, U , on it [23]. Microstate distribution or probability distribution is proportional to Boltzmann factor.

$$\wp_C(N, V, T, \mathbf{r}^N, \boldsymbol{\sigma}^N) \propto e^{-\beta U(\mathbf{r}^N, \boldsymbol{\sigma}^N)} \quad (16)$$

Sampling here involves two trial moves. The first one is the atom displacement which is done by randomly selecting an atom then perturbing its x, y, z coordinates separately, $\mathbf{r}^N \rightarrow \mathbf{r}_{new}^N$. The second one is the transmutation which is done by choosing two different types (spins) of atoms randomly and exchanging their types without changing the composition, $\boldsymbol{\sigma}^N \rightarrow \boldsymbol{\sigma}_{new}^N$. This two trial moves change the potential energy

$$\Delta U = U(\mathbf{r}_{new}^N, \boldsymbol{\sigma}_{new}^N) - U(\mathbf{r}^N, \boldsymbol{\sigma}^N) \quad (17)$$

Therefore, according to **Metropolis criterion**, the acceptance probability is

$$P_C^{acc} = \min[1, e^{-\beta \Delta U(\mathbf{r}^N, \boldsymbol{\sigma}^N)}] \quad (18)$$

If ΔU is negative move is accepted with $P^{acc} = 1$, otherwise, $P_c^{acc} = e^{-\beta\Delta U(\mathbf{r}^N, \boldsymbol{\sigma}^N)}$ is computed and compared to a randomly drawn number from the interval $q = [0,1)$. If $P_c^{acc} > q$, the move is accepted with that P^{acc} . For the accepted moves the new configuration is kept and the averages associated with it are updated, while for the rejected moves, the original configuration is kept and the averages associated with it are updated.

1.3.2 Semi-grand canonical ensemble (constant $N, V, T, \Delta\mu$):

SGC ensemble describes a system of constant volume consists of constant number of atoms of each type and is in contact with an infinite reservoir at constant temperature and chemical potential of each atom. Sampling in this ensemble allows to equilibrate the system into different microstates with different compositions, but their average is constrained by the reservoir through the constant $\Delta\mu$. The partition function of this ensemble is given by

$$\mathbb{Q}_{SGC}(N, V, T) = \int_0^1 \mathbb{Q}_C(N, V, T) e^{(-\beta\Delta\mu Nc)} dc \quad (19)$$

The probability distribution of SGC ensemble is given by

$$\wp_{SGC}(N, V, T, \Delta\mu, \mathbf{r}^N, \boldsymbol{\sigma}^N) \propto e^{-\beta[U(\mathbf{r}^N, \boldsymbol{\sigma}^N) + \Delta\mu N\hat{c}(\boldsymbol{\sigma}^N)]} \quad (20)$$

where $\hat{c} = \frac{1}{N} \sum_1^N \sigma_i$ is the concentration of spin (type) 1 atom.

Sampling in SGC using MC transmutations can be described as follows:

- a. an atom is chosen at random.
- b. its type is changed $\boldsymbol{\sigma}^N \rightarrow \boldsymbol{\sigma}_{new}^N$
- c. the energy change, ΔU , is calculated
- d. the change in concentration, $\Delta c = \hat{c}(\boldsymbol{\sigma}_{new}^N) - \hat{c}(\boldsymbol{\sigma}^N)$, is calculated

e. This exchange is accepted or rejected according to the acceptance probability

$$P_{SGC}^{acc} = \min[1, e^{-\beta(\Delta U + \Delta\mu N\Delta c)}] \quad (21)$$

It can be concluded from the acceptance probability, that SGC ensemble cannot be used to establish equilibrium in multiphase fields for the concentration inside these fields cannot be stabilized and this is attributed to the fact that $\Delta\mu$ is a function in one average concentration only. This is displayed as a jump or discontinuity in concentration in the $\Delta\mu - \langle\hat{c}\rangle$ plot.

1.3.3 Variance-constrained semi-grand canonical ensemble:

As discussed above SGC ensemble can be used to establish equilibrium in single phase systems where the concentration can be stabilized by $\Delta\mu$. On the other hand, SGC ensemble cannot be used with two-phase fields where the relation between the average concentration and the potential difference has infinite slope [42]. To render SGC applicable in two-phase fields, more constraints need to be used to stabilize the global composition at the value of interest [42]. This can be achieved by adding two independent parameters, ϕ and κ , that control the reservoir of VC-SGC [43]. AS compared to SGC ensemble, where $\Delta\mu$ is the Lagrange multiplier that constrains global concentration, two additional Lagrange multipliers, ϕ and κ are added to constrain the global concentration in VC-SGC ensemble. The partition function of this ensemble is given by

$$\mathbb{Q}_{VC-SGC}(N, V, T) = \int_0^1 \mathbb{Q}_C(N, V, T) e^{-\beta N c(\phi + \kappa N c)} dc \quad (22)$$

The probability distribution of VC-SGC ensemble is given by

$$\wp_{VC-SGC}(N, V, T, \phi, \kappa, \mathbf{r}^N, \boldsymbol{\sigma}^N) \propto e^{-\beta[U(\mathbf{r}^N, \boldsymbol{\sigma}^N) - \beta\kappa(\phi/2\kappa + N\hat{c}(\boldsymbol{\sigma}^N))^2]} \quad (23)$$

The acceptance probability of the variance-constrained semi-grand canonical (VC-SGC) ensemble is

$$P_{VC-SGC}^{acc} = \min[1, e^{-\beta(\Delta U + N\Delta c(\phi + 2\kappa N\tilde{c}))}] \quad (24)$$

where \tilde{c} is the average concentration between two successive trial moves. The algorithm was implemented in the massively parallel MD code LAMMPS [23].

1.4 Density Functional Theory:

A system of a solid containing very large number of atoms ($\sim 10^{23}$) and multiple numbers of electrons can theoretically be described exactly with the following Hamiltonian in atomic units. The Spin dependence is not shown here for clarity.

$$\hat{H} = -\frac{1}{2} \sum_I^N \nabla_I^2 - \frac{1}{2} \sum_i^n \nabla_i^2 + \frac{1}{2} \sum_{J \neq I}^N \frac{Z_I Z_J}{|\mathbf{R}_I - \mathbf{R}_J|} + \frac{1}{2} \sum_{j \neq i}^N \frac{1}{|\mathbf{r}_i - \mathbf{r}_j|} - \sum_{I=1}^N \sum_{i=1}^n \frac{Z_I}{|\mathbf{R}_I - \mathbf{r}_i|} \quad (25)$$

N here represents the number of nuclei with the mass M and n the number of interacting electrons with mass m . \mathbf{R}_I and \mathbf{r}_i designate their positions and Z_I is the associated atomic number, which indicates the multiplicity of the elementary charge e . The first two terms describe the kinetic energy of the nuclei and the electrons. The third and fourth terms describe the Coulombic interaction between the nuclei and the electrons respectively. The last term describes the Coulombic interaction between the nuclei and the electrons. In principle, if all these terms are known, then the corresponding Many-Body Schrödinger equation, **Equation (26)**, can be solved.

$$\hat{H}\Psi(\{\mathbf{r}_i\}, \{\mathbf{R}_J\}) = E\Psi(\{\mathbf{r}_i\}, \{\mathbf{R}_J\}) \quad (26)$$

In practice, this is not possible, for the equation is partial differential equation in $3(N + n)$ variables. A first simplification of the Hamiltonians is provided by the Born-Oppenheimer

approximation [44]. Because the inertia of the nucleus is much larger than that of the electron, the nucleus can be considered stationary, hence the electronic and nuclear dynamics can be decoupled. The Hamiltonian in **Equation (26)**, becomes the n-electron Hamiltonian of the stationary lattice.

$$\hat{H} = \underbrace{-\frac{1}{2} \sum_i^n \nabla_i^2}_{\hat{T}} + \underbrace{\frac{1}{2} \sum_{j \neq i}^N \frac{1}{|\mathbf{r}_i - \mathbf{r}_j|}}_{\hat{V}_{ee}} - \underbrace{\sum_{I=1}^N \sum_{i=1}^n \frac{Z_I}{|\mathbf{R}_I - \mathbf{r}_i|}}_{\hat{V}_{ext}} \quad (27)$$

The corresponding Schrödinger equation is

$$\hat{H}\Psi(\mathbf{r}_i) = E\Psi(\mathbf{r}_i) \quad (28)$$

The solution of this equation gives the energy eigenvalues of the ground and all the excited states. Carrying this out for many different nuclei positions, one can get the energy hypersurface for every electronic state. From the global minimum of the hypersurface of the ground state which corresponds to the most stable structure, lattice parameter, cohesive energy and other properties can be calculated. Further calculation such as band structure, density of states can be made starting from this ground state configuration. But the solution of this equation is still problematic since the second term couples the electronic coordinates and makes **Equation (27)** yet complicated partial differential equation in $3(n)$ variables.

Hartree approximation [45], *mean field approach*, simplified the n-electron Schrödinger equation by treating the electron as independent non-interacting electrons. In this approximation, each electron recognizes the other electrons as a mean field Coulombic potential due to the other $(n - 1)$ electrons. The $(n - 1)$ electrons are treated as smooth negative charge density, at a position defined by $\hat{\mathbf{r}}$, that creates a potential, *Hartree potential*, of the following form

$$V_H(\mathbf{r}) = \int \rho(\hat{\mathbf{r}}) \frac{1}{|\mathbf{r} - \hat{\mathbf{r}}|} d\hat{\mathbf{r}}, \quad E_H = \frac{1}{2} \int \int \frac{\rho(\mathbf{r})\rho(\hat{\mathbf{r}})}{|\mathbf{r} - \hat{\mathbf{r}}|} d\mathbf{r} d\hat{\mathbf{r}} \quad , \quad \rho(\hat{\mathbf{r}}) = \sum_i |\Psi_i(\hat{\mathbf{r}})|^2 \quad (29)$$

hence decoupling the electronic coordinates and rendering the n -electron Schrödinger equation into n one-electron Schrödinger equation

$$\Psi(\mathbf{r}_1, \mathbf{r}_1, \dots, \mathbf{r}_n) = \psi_1(\mathbf{r}_1) \psi_2(\mathbf{r}_2) \dots \psi_n(\mathbf{r}_n) \quad (30)$$

1.4.1 The Hohenberg-Kohn theorems:

In 1964, Pierre Hohenberg and Walter Kohn [46] showed that the electronic ground state can be defined by the electronic Density $\rho(\mathbf{r})$, thus laying the foundation for density functional theory (DFT). The Hohenberg-Kohn theorems are related to any system consisting of electrons moving under the influence of an external potential V_{ext} .

The *first theorem* states that:

The external potential V_{ext} (and hence the total energy), is a unique functional of the electronic density $\rho(\mathbf{r})$ [46].

The relation between the electron density $\rho(\mathbf{r})$ and the external potential V_{ext} can be qualitatively deduced from the following facts:

- The electronic density depends on the position coordinates.
- Integration of all the electron densities over the whole space gives the total number of the electrons which interact with the nucleus

$$\int \rho(\mathbf{r}) d\mathbf{r} = n \quad (31)$$

- The mean electron density at the position of the nucleus, A , contains information about the charge of the nucleus, Z , as shown in **Figure 1.1**.

$$\left. \frac{\partial \bar{\rho}(\mathbf{r})}{\partial r} \right|_{r=r_A} = -2Z_A \bar{\rho}(\mathbf{r}_A) \quad (32)$$

- The electronic density decays exponentially at large distances from the nucleus.

$$\rho(\mathbf{r}) \sim e^{-(2\sqrt{2I}|\mathbf{r}|)}$$

where I is the exact ionization energy of the system.

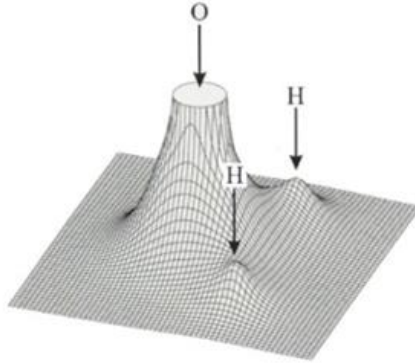


Figure 1.1 Electron density for water molecule

The total energy is then can be described as a functional of electron density

$$E[\rho(\mathbf{r})] = E_{kin}[\rho(\mathbf{r})] + E_{ext}[\rho(\mathbf{r})] + E_H[\rho(\mathbf{r})] + E_{XC}[\rho(\mathbf{r})] \quad (33)$$

$$E[\rho(\mathbf{r})] = \underbrace{-\frac{1}{2} \sum_i \int \varphi_i^* \nabla^2 \varphi_i d\mathbf{r}}_{E_{kin}} - \underbrace{\int \rho(\mathbf{r}) V_{ext}(\mathbf{r}) d\mathbf{r}}_{E_{ext}} + \underbrace{\frac{1}{2} \iint \frac{\rho(\mathbf{r})\rho(\mathbf{r}')}{|\mathbf{r}-\mathbf{r}'|} d\mathbf{r} d\mathbf{r}'}_{E_H} + E_{XC}[\rho(\mathbf{r})] \quad (34)$$

and $\rho(\mathbf{r}) = \sum_i |\varphi_i(\mathbf{r})|^2$, where $\varphi_i(\mathbf{r})$ are the non-interacting Kohn-Sham orbitals that replace the eigenfunctions of the interacting electrons. $F[\rho(\mathbf{r})] = E_{kin}[\rho(\mathbf{r})] + E_H[\rho(\mathbf{r})] + E_{XC}[\rho(\mathbf{r})]$ where the terms are the kinetic energy of the electrons, Hartree Energy, and exchange-correlation energy respectively. As opposed to the external potential, V_{ext} , which varies from one system to another, $F[\rho(\mathbf{r})]$ does not.

$E_{XC}[\rho(\mathbf{r})]$, as expected, is not so easy to define because it contains corrections to self-interaction and contains other (quantum mechanical) effects that are missing due to using the electron density and the decoupling of electron coordinates. Strictly speaking, the exact form of the exchange-correlation functional, even if its existence is required and proved by the Hohenberg-Kohn theorems, is unknown as the other terms.

$$E_{XC}[\rho(\mathbf{r})] = E_X[\rho(\mathbf{r})] + E_C[\rho(\mathbf{r})] \quad (35)$$

$E_X[\rho(\mathbf{r})]$ is the exchange energy which is attributed to Pauli exclusion principle that makes the like-spin electrons avoid each other, hence staying at a distance from each other. This reduces the electron density around the electron (hence creating what so called exchange hole) and the net repulsive energy, hence the $E_X[\rho(\mathbf{r})]$ has negative value. $E_C[\rho(\mathbf{r})]$ is the correlation energy and comprises all the interacting terms that are not accounted for because of the decoupling of the coordinates of the electrons. Electrons of different spins repel each other on the same orbital that they occupy, because they have the same charge, hence creating correlation holes around the electrons and reduce the net repulsive energy. $E_C[\rho(\mathbf{r})]$ has a negative value and it is much less than the exchange energy.

There is only one special case from which the functional can be derived exactly. This is when the electron density is constant, $\rho(\mathbf{r}) = \text{const.}$ i. e. it has the same value at every point in the space. One speaks also of a homogeneous electron gas. This situation may be limited in practical applications, as electrons are rarely uniformly distributed. This approach can be applied to simple metals (Alkali metals like Li, Na, K). The first approach to approximate the exchange correlation energy is the *Local Density Approximation* (LDA), which initially assumes that there is a

homogeneous electron gas. In this case, $E_{XC}[\rho(\mathbf{r})]$ is a pure functional of density and can be split into an exchange term $E_X[\rho(\mathbf{r})]$ and a correlation term $E_C[\rho(\mathbf{r})]$. The exchange term is given by

$$E_X^{LDA}[\rho(\mathbf{r})] = \int d\mathbf{r} \rho(\mathbf{r}) \epsilon_X^{LDA}[\rho(\mathbf{r})]$$

$$\epsilon_X^{LDA}[\rho(\mathbf{r})] = -\frac{3}{4} \left(\frac{3}{\pi}\right)^{1/3} \rho(\mathbf{r})^{1/3}$$

The correlation term is given by

$$E_C^{LDA}[\rho(\mathbf{r})] = \int d\mathbf{r} \rho(\mathbf{r}) \epsilon_C^{LDA}[\rho(\mathbf{r})]$$

$$\epsilon_C^{LDA}[\rho(\mathbf{r})] = A \left\{ \ln\left(\frac{x^2}{X}\right) + \frac{2b}{Q} \tan^{-1}\left(\frac{Q}{2x+b}\right) - \frac{bx_o}{X(x_o)} \left[\ln\left(\frac{(x-x_o)^2}{X}\right) + \frac{2(b2x_o)}{Q} \tan^{-1}\left(\frac{Q}{2x+b}\right) \right] \right\}$$

$$X = x^2 + bx + c, \quad x = \sqrt{r_s}, \quad r_s = \sqrt[3]{\frac{3}{4\pi\rho(r)}}, \quad Q = \sqrt{4c - b^2}, \quad x_o = -0.104098,$$

$$A = 0.0310907, \quad b = 3.72744, \quad c = 12.9352$$

As already mentioned, this approximation works well for substances with approximately homogeneous electron density, for example, metals. However, it turns out that this approximation leads to good results with other materials as well. Only for chemical problems is the local density approximation too imprecise, as it tends to give too high binding energies and too low ground state energies.

For this reason, various improvements have been made. One of these improvements is the **Generalized Gradient Approximation** (GGA), in which the functionals depend not only on the density $\rho(\mathbf{r})$ but also on the gradient $\nabla\rho(\mathbf{r})$

$$E_X^{GGA}[\rho(\mathbf{r}), \nabla\rho(\mathbf{r})] = \int d\mathbf{r} \rho(\mathbf{r}) \epsilon_X^{GGA}[\rho(\mathbf{r}), \nabla\rho(\mathbf{r})]$$

$$E_C^{GGA}[\rho(\mathbf{r}), \nabla\rho(\mathbf{r})] = \int d\mathbf{r} \rho(\mathbf{r}) \epsilon_C^{GGA}[\rho(\mathbf{r}), \nabla\rho(\mathbf{r})]$$

The exact expressions are not given here because they are even more complicated and longer than the *LDA*. Only known names for these functionals can be given: Perdew-Wang-Funktional (PW91) [47], Perdew-Burke-Ernzerhof-Funktional (PBE) [48].

The *second theorem* states that:

The electron density that minimizes the energy functional is the one that *gives the lowest energy if and only if the input density is the true ground state density* [46].

This is realized in practice by using the variational principle method.

$$\frac{\delta E [\rho(\mathbf{r})]}{\delta \rho(\mathbf{r})} = 0 \quad (36)$$

This is done by varying the electron density until the approximate form of the functional, that describes the ground state energy becomes minimal. The resulting electron density is then the relevant ground state density.

1.4.2 Kohn-Sham equations:

The Kohn-Sham equations have the following form:

$$\left[-\frac{1}{2}\nabla^2 + V_{eff}(\mathbf{r}) \right] \varphi_i(\mathbf{r}) = \epsilon_i \varphi_i(\mathbf{r}) \quad (37)$$

$V_{eff}(\mathbf{r})$ is the effective potential and is given by

$$V_{eff}(\mathbf{r}) = V_{ext}(\mathbf{r}) + V_H(\mathbf{r}) + V_{XC}(\mathbf{r}) \quad (38)$$

The first term is the external potential and is proportional to $\frac{Z}{r}$, the second term is Hartree potential, and the third one is the exchange-correlation potential functional. Now **Equation (38)** becomes

$$\left[-\frac{1}{2}\nabla^2 + V_{ext}(\mathbf{r}) + V_H(\mathbf{r}) + V_{XC}(\mathbf{r}) \right] \varphi_i(\mathbf{r}) = \epsilon_i \varphi_i(\mathbf{r}) \quad (39)$$

and the corresponding total energy functional is

$$E[\rho(\mathbf{r})] = \underbrace{-\frac{1}{2} \sum_i \int \varphi_i^* \nabla^2 \varphi_i d\mathbf{r}}_{E_{kin}} - \underbrace{\sum_{I=1}^N \int \frac{Z_I \rho(\mathbf{r})}{|\mathbf{r} - \mathbf{R}_I|} d\mathbf{r}}_{E_{ext}} + \underbrace{\frac{1}{2} \int \int \frac{\rho(\mathbf{r}) \rho(\mathbf{r}')}{|\mathbf{r} - \mathbf{r}'|} d\mathbf{r} d\mathbf{r}'}_{E_H} + E_{XC}[\rho(\mathbf{r})] \quad (40)$$

The Kohn-Sham equations are solved using the **self-consistent procedure** as follows:

- 1- A trial electron density, $\rho(\mathbf{r})$, is calculated.
- 2- $V_{XC}(\mathbf{r})$ is calculated along with the other terms of the **Kohn-Sham** Hamiltonian.
- 3- The set of equation are solved, and the solutions are **Kohn-Sham** orbitals $\varphi_i(\mathbf{r})$.
- 4- The **Kohn-Sham** orbitals $\varphi_i(\mathbf{r})$ are used to calculate a new $\rho(\mathbf{r})$. The previous and the new electron densities are mixed, and all the previous steps are repeated with the mixed electron density.
- 5- When the energy change or electron density change is small enough (usually about 10^{-8} Ry), the obtained energy is the *ground state energy* and the electron density is the ground state electron density.

1.4.3 The pseudopotential:

A reduction in the computational effort in quantum calculations in solids can be achieved by explicitly considering only the valence electrons in the solution of the Schrödinger equation (Frozen-core approximation). For example, in Platinum, there are 10 valence electrons out of total 78 electrons, and this reduces the computational cost by $\sim 87\%$. This approximation is possible because the core electrons hardly contribute, as opposed to valence, to chemical bonds; therefore, core electrons are frozen and treated with the nuclei as one rigid ion core.

The pseudopotential is an effective potential, in which only the valence electrons are involved, to replace the full-potential (All-Electron potential), and valence electrons are described by pseudo-wavefunctions accordingly. The corresponding Schrödinger equation is modified with this effective potential term instead of the usual Coulombic potential term that normally considers core electrons, see **Figure 1.2**.

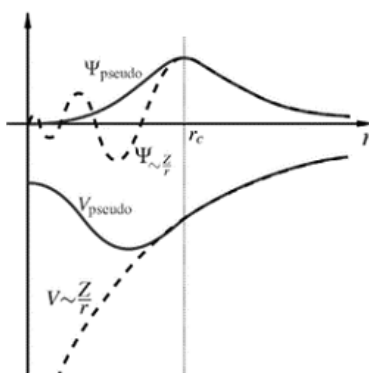


Figure 1.2 The construction of pseudopotential

To construct the pseudopotential, an atomic is used as reference state, to make it applicable to different systems. Then making the pseudo-valence ψ_i^{PP} and All-Electron ψ_i^{AE} wavefunctions have the same energies and amplitude (and thus electronic density) at a properly chosen core cut-

off radius r_c . The initial trial electron density used in the **self-consistent procedure** is calculated from superposition of pseudo-valence wavefunctions.

$$\rho(\mathbf{r}) = \sum_i |\psi_i^{PP}(\mathbf{r})|^2 \quad (41)$$

Examples of the types of pseudopotentials are *Soft* and *Ultrasoft* pseudopotentials, *Norm-conserving* pseudopotentials, and *Projector-Augmented Wave* (PAW).

1.4.4 Electrons in solids:

Free electrons have wavefunctions of a form of a traveling planewave PW.

$$\Psi(\mathbf{r}) = e^{i\mathbf{k}\cdot\mathbf{r}} \quad (42)$$

where \mathbf{k} is the wavevector. However, in the solids that display a periodic crystal structure, the electron is not completely free, and it travels inside the solid as a traveling planewave that is modulated with a function that has the periodicity of the crystal structure $u_k(\mathbf{r})$.

$$\Psi(\mathbf{r}) = u_k(\mathbf{r})e^{i\mathbf{k}\cdot\mathbf{r}}, \quad u_k(\mathbf{r}) = u_k(\mathbf{r} + \mathbf{R}) \quad (43)$$

where \mathbf{R} is the translation vector in the real space. The periodic function $u_k(\mathbf{r})$, however, can be expanded in the reciprocal space (Fourier space).

$$u_k(\mathbf{r}) = \sum_{\mathbf{G}} c_k(\mathbf{G})e^{i\mathbf{G}\cdot\mathbf{r}} \quad (44)$$

where \mathbf{G} is the reciprocal space vector. Substituting **Equation(44)** in **Equation (43)** yields what so called **Bloch wave**.

$$\Psi_{\mathbf{k}}(\mathbf{r}) = \sum_{\mathbf{G}} c_{\mathbf{k}}(\mathbf{G}) e^{i(\mathbf{k}+\mathbf{G})\cdot\mathbf{r}} \quad (45)$$

Bloch wave is a superposition of planewaves with wavevector \mathbf{k} (in the first Brillouin zone), that differ by a reciprocal vector \mathbf{G} . The number of electronic states, \mathbf{k} s, can be reduced by using supercells and the concept of periodic boundary conditions; and by reducing the **first Brillouin zone** using symmetry operations (inversion and rotation) to the **irreducible Brillouin zone (IBZ)** as shown in **Figure 1.3**.

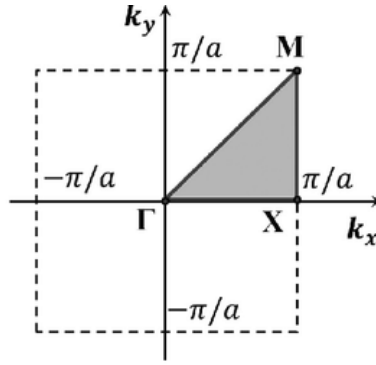


Figure 1.3 The irreducible Brillouin zone (IBZ).

$V_{eff}(\mathbf{r})$ is also periodic in the real space and can be expanded in the reciprocal space (Fourier space) as

$$V_{eff}(\mathbf{r}) = \sum_{\mathbf{G}} V_{eff}(\mathbf{G}) e^{i\mathbf{G}\cdot\mathbf{r}} \quad (46)$$

$$V_{eff}(\mathbf{G}) = \int V_{eff}(\mathbf{r}) e^{i\mathbf{G}\cdot\mathbf{r}} d\mathbf{r} \quad (47)$$

Plugging **Equation(45)** and **Equation(46)** in **Equation(37)** with some manipulation yields the KS equations in the reciprocal space

$$\sum_{\mathbf{G}'} \left[\frac{1}{2} |\mathbf{k} + \mathbf{G}'|^2 + V_{eff}(\mathbf{G} - \mathbf{G}') \right] c_n(\mathbf{k} + \mathbf{G}') = \epsilon_{nk} c_n(\mathbf{k} + \mathbf{G}) \quad (48)$$

Or in matrix form $\mathbf{H}\mathbf{c} = \epsilon\mathbf{c}$

where n is the energy band index. This matrix can be solved for a fixed band index and for the basis set of planewaves by diagonalization and the obtained $c_n(\mathbf{k} + \mathbf{G})$ are used to calculate new KS orbitals φ_{nk} which are used to calculate the new electron density and the KS Hamiltonian as described in the self-consistent procedure.

To expand the wavefunction and describe it precisely, an infinite number of PWs are required and this would make solving **Equation(48)** impossible. Since the target energy is the ground state energy, then the important solutions are the ones with the lowest energies. This can be done by excluding the electrons with the highest kinetic energy by introducing a *cutoff-energy*, E_{cut} .

$$E_{cut} \geq \frac{1}{2} |\mathbf{k} + \mathbf{G}|^2 \quad (49)$$

The E_{cut} is system-dependent and a convergence test must be carried out until the energy or other properties do not change.

Chapter 2: Molecular Dynamics and Hybrid MD/MC Computations:

2.1 Computational procedure:

The massively parallel MD code LAMMPS was used to perform Hybrid MC/MD simulations [42]. To choose the proper potential that represents the rich side of Al-Cu system, four interatomic potentials were compared in terms of the formation energies of four different intermetallic compounds and the results are shown in **Table 1.1**. The best results (green column) obtained by the embedded-atom (EAM)interatomic potential that was developed by W. Sheng [49].

Potential	Adp ⁵⁰	MEAM ⁵¹	EAM (AlCu) ⁵²	EAM (CuAl) ⁴⁹	Ab initio
AlCu ₃ (D0 ₂₂)	-0.245	-0.017	-0.123	-0.197	0.185 ⁵³
AlCu ₃ (D0 ₃)	-0.272	-0.094	-0.153	-0.170	0.169 ⁵³
AlCu ₃ (L1 ₂)	-0.162	0.284	-0.155	-0.194	-0.182 ⁵⁴
Al ₄ Cu ₉ (D8 ₃)	-0.331	-0.038	-0.151	-0.207	0.215 ⁵³

Table 2.1 Comparison of four different interatomic potentials in terms of formation energy

The simulations were run using three different starting states at 300K, namely Cu ($a=3.615 \text{ \AA}$), Al ($a=4.05 \text{ \AA}$), and Al₄Cu₉ (γ phase, $a=8.701 \text{ \AA}$). The simulation box of the FCC lattices was cubic supercell, 5x5x5 unit cells, which employed 500 atoms, while that for (γ phase) was orthorhombic supercell, 5x2x1, which employed 520 atoms. The simulation was also run at 700K and 1000K starting from Cu supercell. In all the simulations, periodic boundary conditions were used in all directions to treat the samples as infinite bulks.

The potential energy of all the starting states samples were minimized using conjugated gradient minimization method. To ensure that each system is relaxed, a constant NPT MD simulation was carried out under P=0 bar for 2 ns using timestep of 1 fs, which is equivalent to 2E6 simulation steps, by annealing each system from a higher temperature to the intended

production temperature, 300, 700, and 1000K; it was 1000K for the 300 and 700K cases, and 1300K for 1000K case. This is done to ensure that each system can visit as many microstates as possible that cannot be visited otherwise, and to identify the microstate with a global minimum. Each system was further equilibrated at the production temperature for 3 ns, which is equivalent to 3E6 simulation steps. After that, the alloying stage was simulated using the MC/MD hybrid method in SGC ensemble [42]. Here each system was first relaxed using conjugated gradient minimization method, then simulation was run for 5E6 simulation steps with timestep of 0.2 fs, and MC transmutations and trial moves was carried out every 500 MD steps, and the fraction of swapped atoms was 0.2. After equilibrium the, the averages were calculated for the last 4000 MC steps (last 2E6 MD steps). During the simulation each simulation $\Delta\mu = \mu_{Cu} - \mu_{Al}$ was kept constant to allow the switching of atomic identities and hence allow the system to reach its corresponding equilibrium concentration. **Figure 2.1** shows schematic representation of the simulation procedure.

Also, simulations were carried out using larger simulation supercells for Cu and γ phase starting states at the same temperatures used in the above simulations. The simulation box of the FCC lattices was cubic supercell, 7x7x7 unit cells, which employed 1372 atoms, while that for (γ phase) was cubic supercell 3x3x3, which employed 1404 atoms. The simulations consist of the same stages as for the smaller supercells. The differences were in the length of the most simulation stages and the fraction of the swapped atoms. The first stage was run for 2E6 steps, then the second stage for 8E6 steps. The last stage, alloying stage, was run for 1E7 steps. The fraction of swapped atoms was 0.3. After equilibrium the, the averages were calculated for the last 4000 MC steps (last 2E6 MD steps).

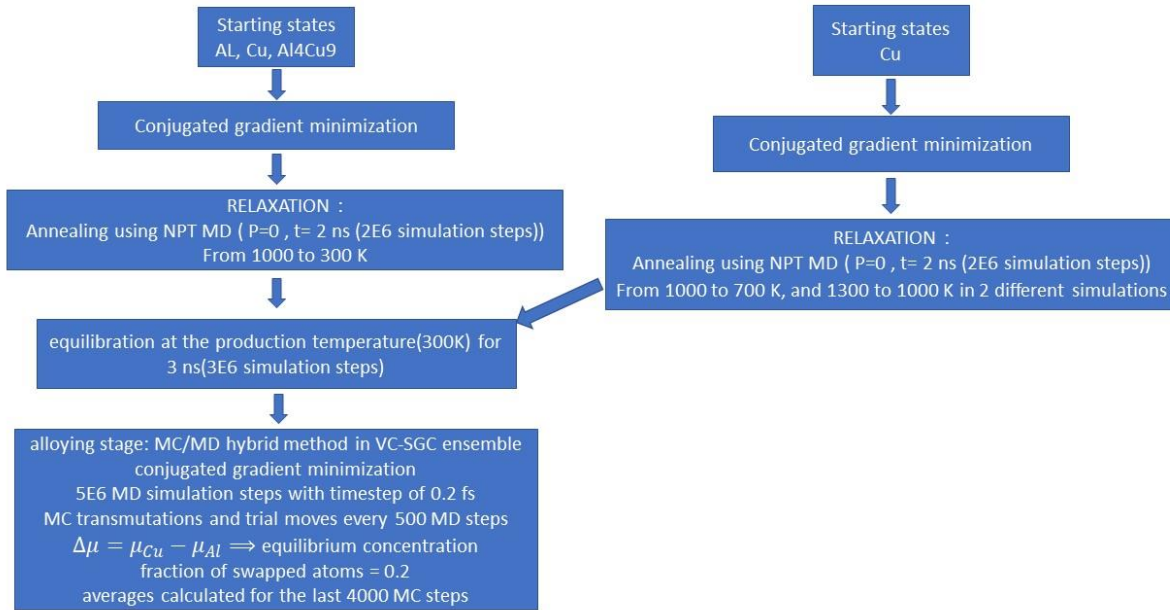


Figure 2.1 Schematic representation of the simulation procedure for the smaller supercells.

The enthalpy of solution was computed for the smaller Cu supercell (500 atoms) using MC/MD canonical ensemble at constant NPT under P=0 bar and T= 300K. The simulation was run from Cu starting state for 5 ns (5E6 steps) and alloying with Al was done at intervals of about 5 at. % up to 20 at%. Al. The rest was done at intervals of about 20 at %.

2.2 Results and discussions:

The plot of equilibrium concentration C_{Cu} (atomic fraction) versus $\Delta\mu$ at each specified temperature was plotted. **Figure 2.2** shows the simulation result of the *smaller supercell Cu starting state for T=300K*. For small values of $\Delta\mu$, the alloy equilibrates into Cu-Al solid solution. With the increase of $\Delta\mu$, the solubility of Al increases and reaches its maximum, 1.6 % (98.4 % Cu), at $\Delta\mu = -0.6125$ eV/atom. At $\Delta\mu = -0.61$, Al concentration increases (jumps) to 22.1

%(77.9 % Cu). The presence of this concentration jump indicates that in this range of composition there are two phases in equilibrium; one certainly is known which the solid solution of Al in Cu is, while the other requires further experimental investigations to reveal its identity.

Figure 2.3 shows the simulation result of the *smaller supercell Al starting state for T=300K*. The change of concentration with $\Delta\mu$ shows the same behavior as for *Cu starting state*, but with slight difference in the extremities of the concentration jump. The jump is between to 1 % (99 % Cu) and 22.3 %(77.7 % Cu) at $\Delta\mu = -0.62$ and respectively. The same behavior is shown by the *smaller supercell Al₄Cu₉ starting state at T=300K* as shown in **Figure 2.4**. The concentration jump occurs between to 0.7 % (99.3 % Cu) and 19.3 %(80.7 % Cu) at $\Delta\mu = -0.66$ and $\Delta\mu = -0.65$.

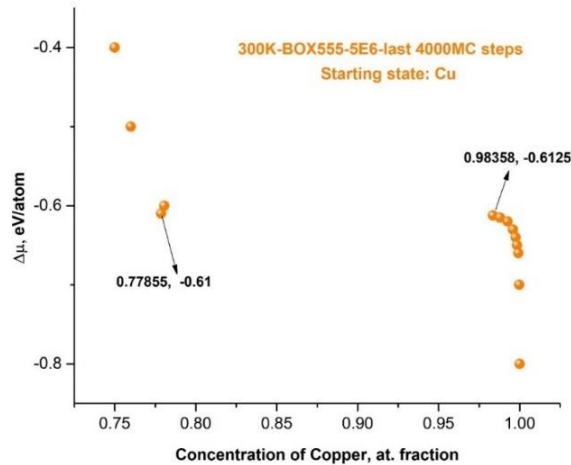


Figure 2.2. Chemical potential difference as a function of concentration for smaller supercell Cu starting state at 300K.

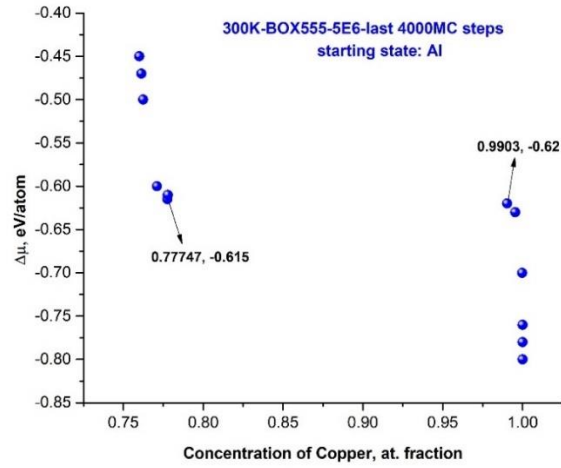


Figure 2.3 Chemical potential difference as a function of concentration for smaller supercell Al starting state at 300K

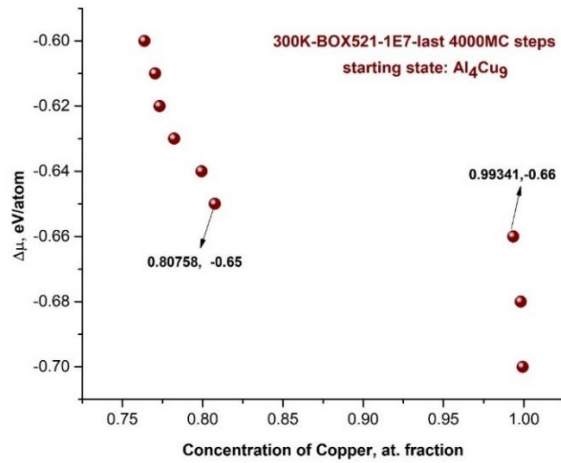


Figure 2.4 Chemical potential difference as a function of concentration for smaller supercell Al4Cu9 starting state at T=300K.

The plot of the concentration C_{Cu} (atomic fraction) versus $\Delta\mu$ for the simulation using the *smaller supercell Cu starting state* at higher temperatures, namely at **700**, and **1000 K** are shown in **Figure 2.5** and **Figure 2.6** respectively. It can be seen from **Figure 2.5** that the alloy equilibrates into Cu-Al solid solution with maximum Al solubility of 14.8 % (85.2 % Cu), where the concentration jump starts, at $\Delta\mu = -0.655$ eV/atom. At $\Delta\mu = -0.65$, Al concentration increases (jumps) to 23.1 % (76.9 % Cu). This makes the two-phase region narrower than at **300 K**.

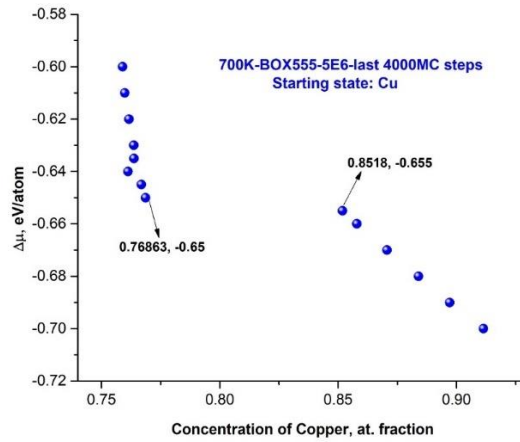


Figure 2.5 Chemical potential difference as a function of concentration for smaller supercell Cu starting state at $T=700\text{K}$

At **1000 K**, as shown in **Figure 2.6**, the concentration jump disappears, which suggests that the solvus line should merge at certain temperature, with the boundary of $(\beta + \text{Cu} - \text{Al})$ two-phase region given that this must satisfy the phase rule. A simulation was carried out at **800 K** to locate where this could occur, and as can be concluded from **Figure 2.7**, the merge should take place between 800 and 1000 K.

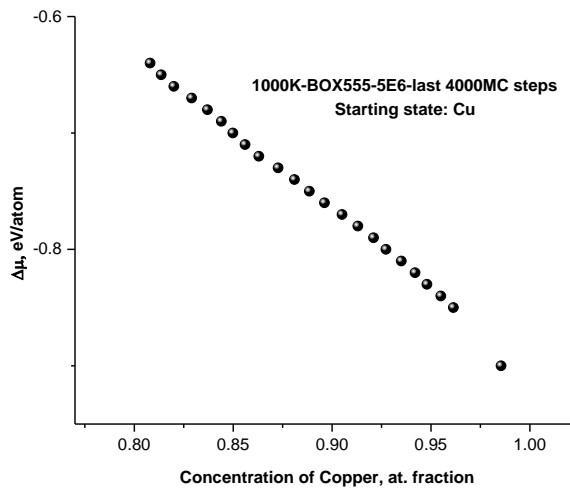


Figure 2.6 Chemical potential difference as a function of concentration for smaller supercell Al_4Cu_9 starting state 1000K.

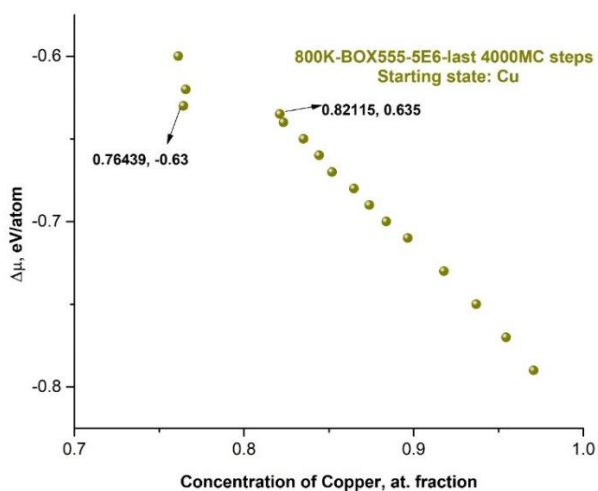


Figure 2.7 Chemical potential difference as a function of concentration for smaller supercell Cu starting state 800K.

For the *larger supercells of Cu starting state*, the plot of equilibrium concentration C_{Cu} (atomic fraction) versus $\Delta\mu$ at 300, 700, 1000 K were plotted, and the results are shown in **Figures 2.8, 2.9, 2.10**. The results confirm that of those for the smaller supercells, but with slight differences in the extremities of the concentration jumps which is attributed to the size of the supercell.

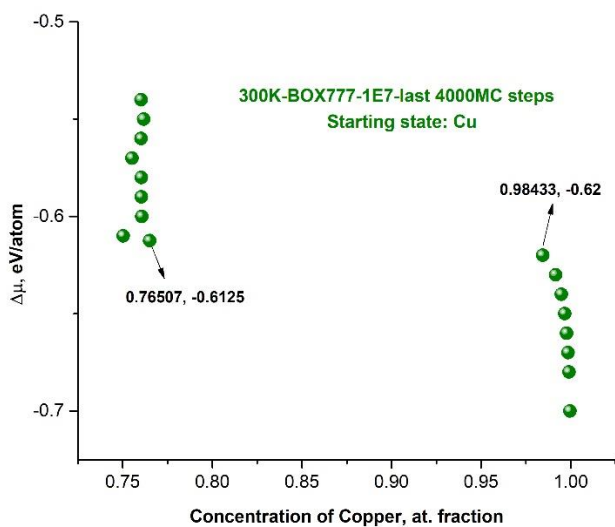


Figure 2.8 Chemical potential difference as a function of concentration for larger supercell Cu starting state at T=300K.

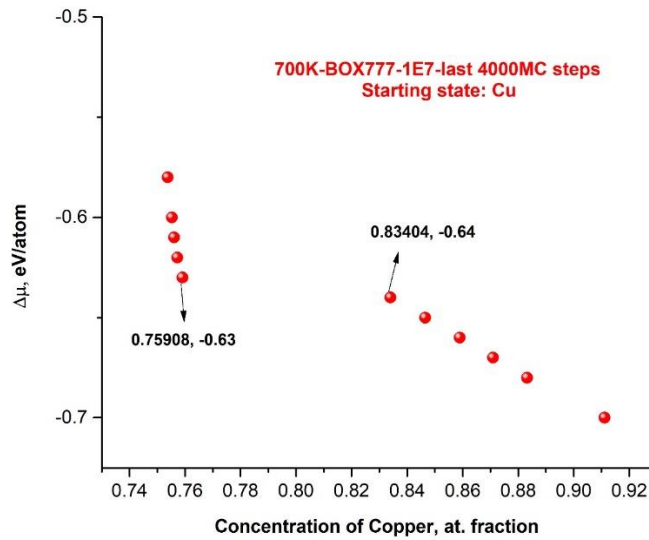


Figure 2.9 Chemical potential difference as a function of concentration for larger supercell Cu starting state at $T=700K$.

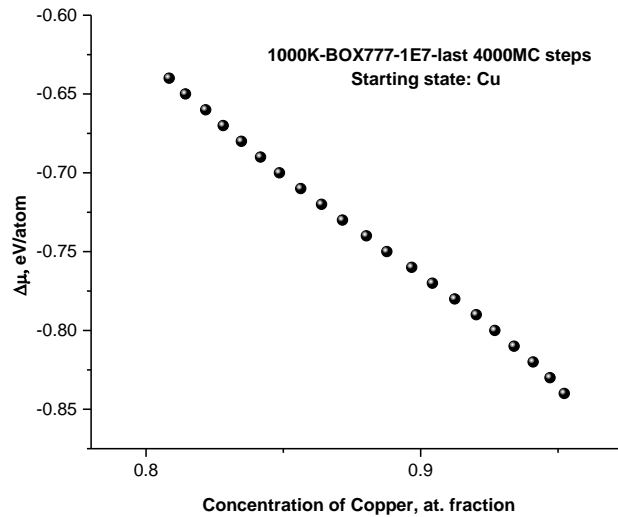


Figure 2.10 Chemical potential difference as a function of concentration for larger supercell Cu starting state at $T=1000K$.

The calculated values of enthalpy of mixing obtained from the simulation that employed smaller supercell Cu starting state at $T=300K$ are plotted and the result is shown in **Figure 2.11**. From that, it can be concluded that the phases in two-phase region are formed by nucleation and growth and not by spinodal decomposition.

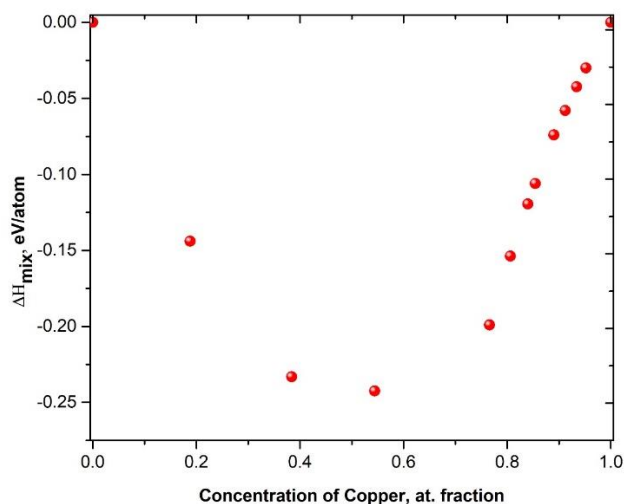


Figure 2.11 Enthalpy of mixing at 300K for smaller supercell Cu starting state

2.2.1 Convergence test:

For the convergence test, an additional Cu supercell of 25000 atoms (25x25x10) was used. The potential energy of the sample was minimized using conjugated gradient minimization method then to ensure that the system is relaxed, a constant NPT MD simulation was carried out under P=0 bar for 0.2 ns from 1000 K to 300 K then using timestep of 1 fs, then at 300K for 0.8 ns. Then the simulation was run using MC/MD semi-grand canonical ensemble at constant NPT under P=0 bar and T= 300K for 1E7 steps with timestep of 0.2 fs, and MC transmutations and trial moves was carried out every 500 MD steps, and the fraction of swapped atoms was 0.2. The averages were taken for the last 4000MC steps. Here, concentration jump took place between (97.974 % Cu, -0.62 eV/atom) and (76.746 % Cu, -0.61 eV/atom). The extremities of concentration jump at 300K for the smaller supercells (500, 1372 atoms) are plotted and the result is shown in **Figure**

2.12. It shows that the concentration jump converges with the size of the supercell which justify the choice of the supercell with 500 atoms for most of the calculations at 300K.

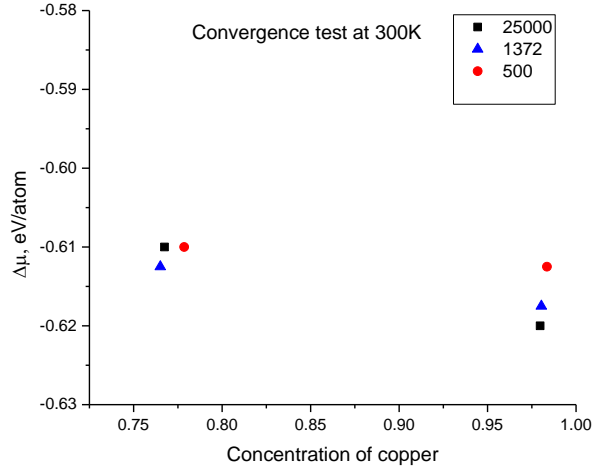


Figure 2.12 Convergence test at 300 K

2.2.2 Visualization results:

The Open Source scientific visualization and analysis software, OVITO, was used to visualize the crystal structure within the 2-phase region. For this purpose, a Cu supercell of 25000 atoms (25x25x10) was used. The potential energy of the sample was minimized using conjugated gradient minimization method then to ensure that the system is relaxed, a constant NPT MD simulation was carried out under P=0 bar for 0.2 ns from 1000 K to 300 K then using timestep of 1 fs, then at 300K for 0.8 ns. The sample then was alloyed randomly by replacing ~0.6 % of Cu atoms with Al atoms. Then the simulation was run using MC/MD canonical ensemble at constant NPT under P=0 bar and T= 300K for 5E5 with timestep of 0.2 fs, and MC transmutations and trial moves was carried out every 500 MD steps, and the fraction of swapped atoms was 0.33. To ensure that equilibrium was reached, the simulation was restarted after the end of the first one under the same condition for 1E5, but MC transmutations and trial moves was carried out every 100 MD steps. **Figure 2.13a** shows the sample just after alloying the sample (α phase). **Figure**

2.13b shows the sample after the initial 5E5 steps (1000MC steps). **Figure 2.13c** shows the sample after the additional 1E5 steps (1000MC steps).

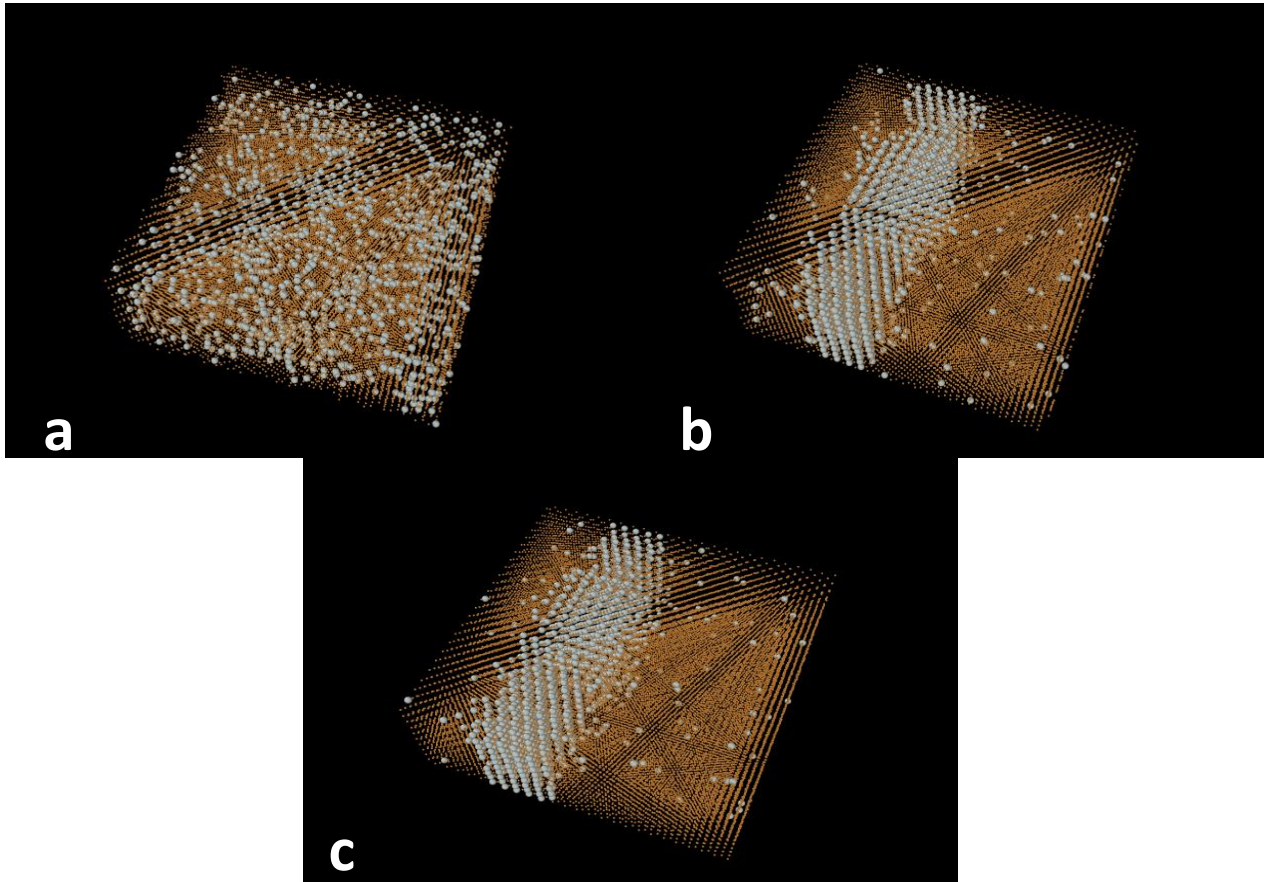


Figure 2.13 Atomic configurations (a) just after alloying the sample (α phase), (b) after the initial 5E5 steps (1000MC steps), (c) after the additional 1E5 steps (1000MC steps).

It is clear from these figures that α phase separated into two phases. According to lever rule the relative amount of α phase (98.36% **Cu**) is

$$\% \alpha \text{ phase} = \frac{94 - 77.86}{98.36 - 77.86} \times 100 = 78.73\%$$

while the relative amount of the other phase (77.86% **Cu**) is 21.27% and this is clear in **Figure 2.13** too. To determine the crystal structure of this phase, four monoatomic slices were cut along [001] direction and the result is shown in **Figure 2.14**. As shown in **Figure 2.14**, two crystal

structures can be identified, one is of $L1_2$ which is outlined with a square in each layer, while the other is $D0_{22}$ and is outlined with a rectangle. **Figure 2.15** shows these two crystal structures.

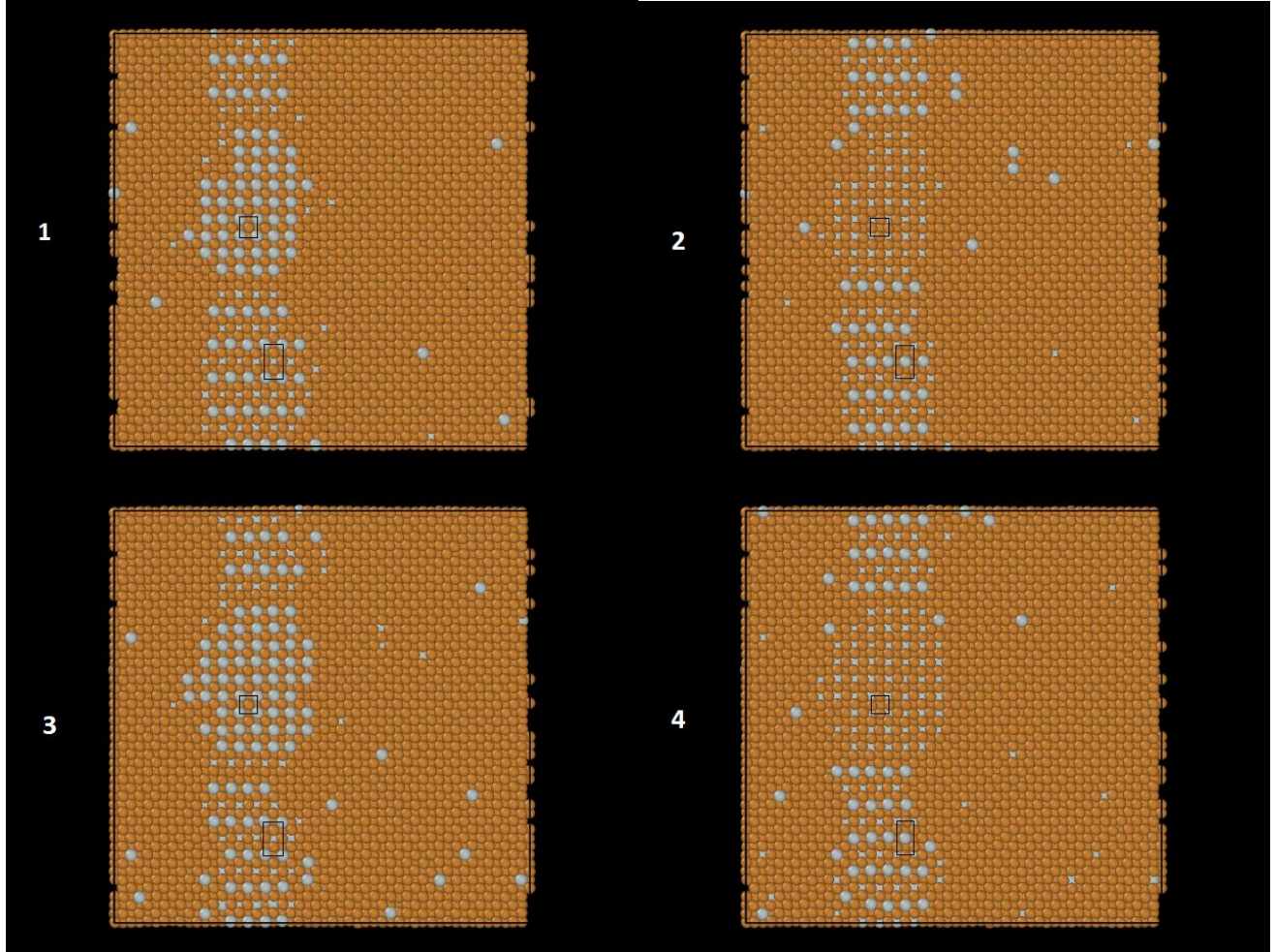


Figure 2.14 The four monoatomic slices cut along $[001]$ direction which shows clearly the $L1_2$, and $D0_{22}$ structures outlined by a square and rectangle respectively.

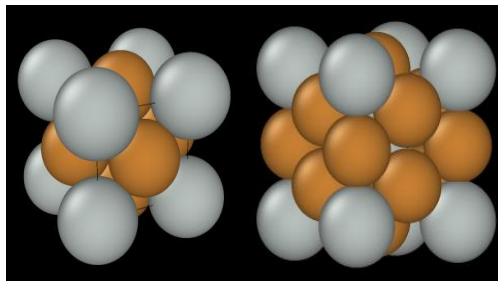


Figure 2.15 $L1_2$ and $D0_{22}$ crystal structures

To have a better look on the crystal structure four monoatomic slices were cut along [010] direction and the result is shown in **Figure 2.16**. It is clear from these monoatomic slices that these two crystal structures are not separate but are one superstructure of $D0_{22}$ and $L1_2$. This suggests that this the α_2 phase which has a long period superstructure of $D0_{22}$ and $L1_2$ [55].

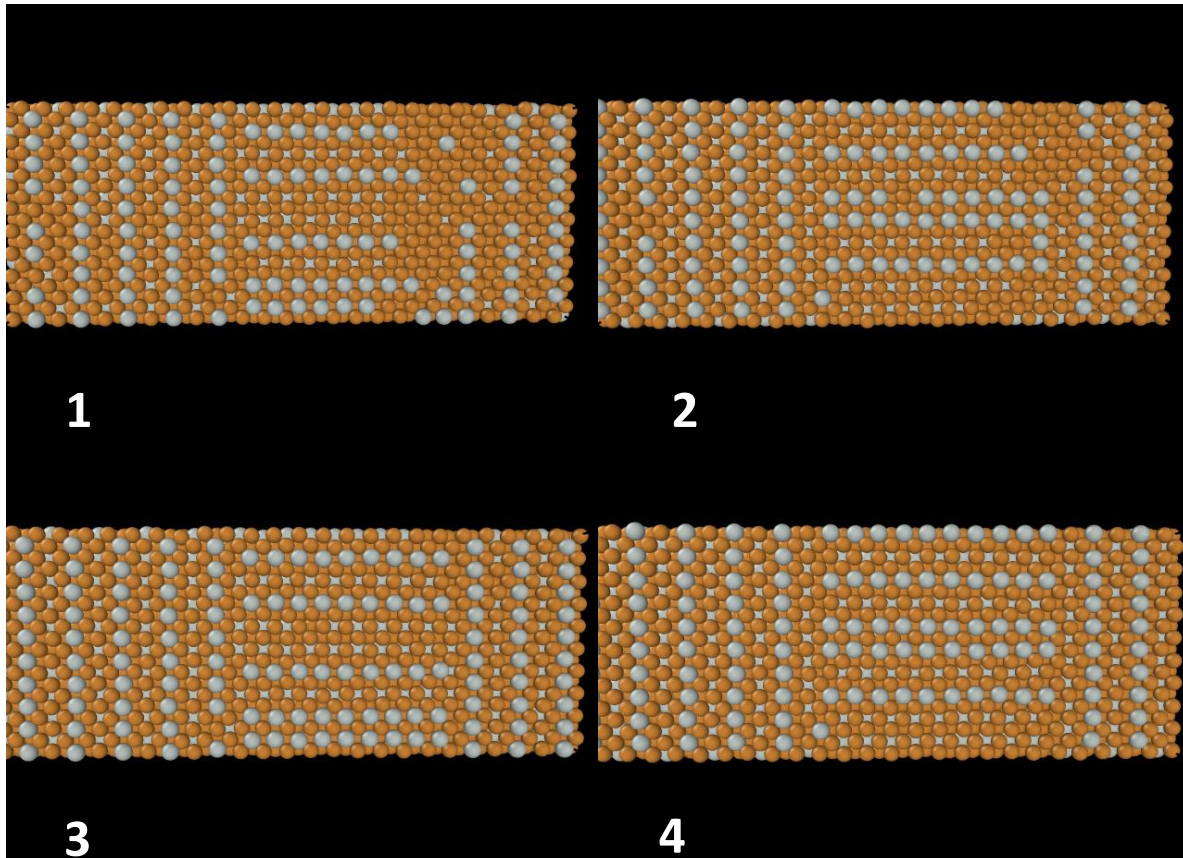


Figure 2.16 The four monoatomic slices cut along [010] direction which show clearly the $L1_2$ and $D0_{22}$ structures

2.2.3 Modification of the Cu-rich side of Al-Cu phase diagram:

The extremities of concentration jump at 300, 700, 800K for the smaller supercells (500 atoms) were plotted, and the result is plotted in **Figure 2.17**. These points are transferred to Al-Cu phase diagram (connected with red lines), as shown in **Figure 2.18**, and possible modifications were drawn such that they obey the phase rule.

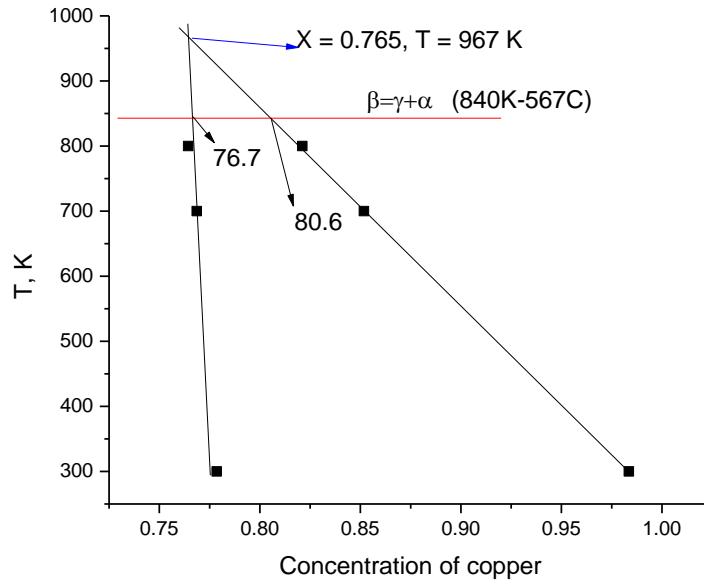


Figure 2.17 The two-phase region is constructed from the extremities of concentration jump at 300, 700, 800K

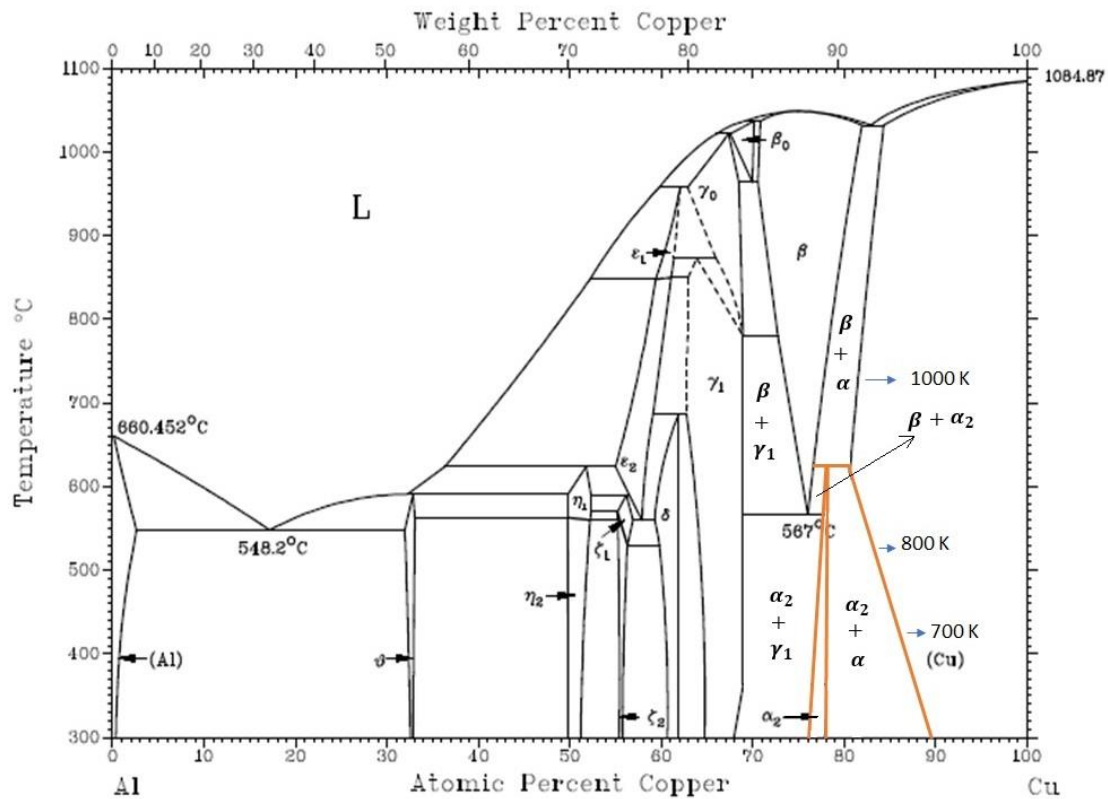
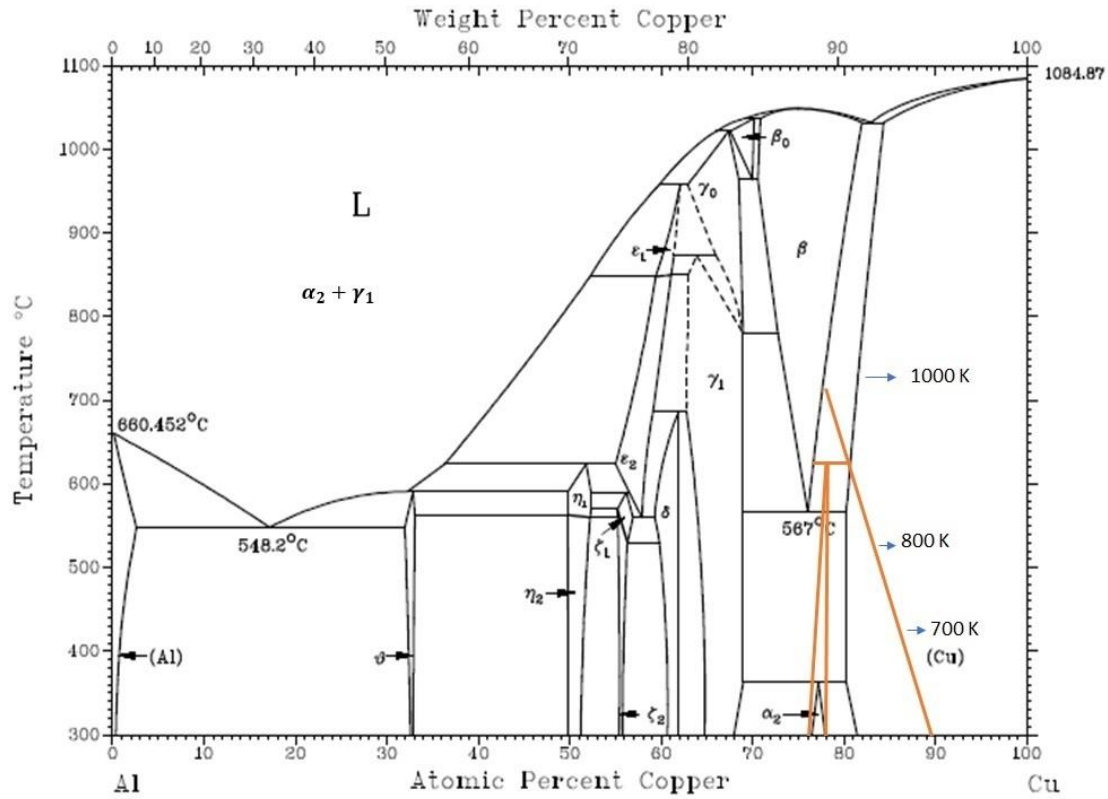


Figure 2.18 Modification of the Cu-rich side of Al-Cu phase diagram

Chapter 3: DFT Computations:

3.1 Computational procedure:

Here, the enthalpy of mixing of two solid solution on the copper-rich side of Al-Cu phase diagram are calculated, namely 6.25% Al and 12.5% Al. The results will be compared to those obtained from molecular dynamics simulations to confirm whether the two phases in the two-phase region formed by nucleation and growth or not.

All calculations were performed in the framework of DFT with the open-source Quantum ESPRESSO package for quantum simulation of materials [56,57]. The projector augmented wave (PAW) method was used throughout the simulations [58,59]. To describe the exchange-correlation energy-functional, the generalized gradient approximation (GGA) [60] formulated by Perdew, Burke and Ernzerhof, [61] was used. Methfessel-Paxton [62] smearing of 0.001 Ry was used throughout the simulations.

3.2 Results and discussion

3.2.1 Aluminum Bulk properties:

For bulk Aluminum, the supercell was one Aluminum FCC unit cell and its corresponding cubic shifted and unshifted k-points grid were used in the simulations. Convergence tests for the supercell with respect to the size of the k-points grid, shifted and unshifted ones, and to cutoff energy, E_{cut} , were carried out and the results were plotted as shown in **Figure 3.1**, and **Figure 3.2** respectively.

As can be seen from **Figure 3.1** the total energy converges better for the shifted k-points grid. The convergence takes place for k-points grid of 10x10x10, but for better precision of the

calculations a shifted 16x16x16 k-points grid of was used. On the other hand, the convergence with respect to energy cutoff takes place at 116 Ry, but an energy cutoff of 250 Ry was used to achieve better results.

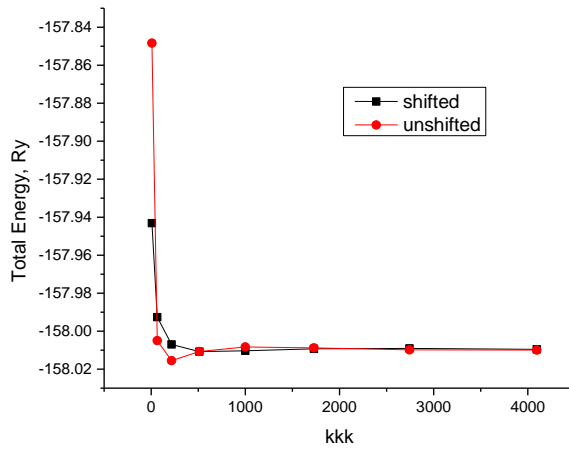


Figure 3.2 Convergence test for bulk Aluminum with respect to unshifted and shifted k-points grids

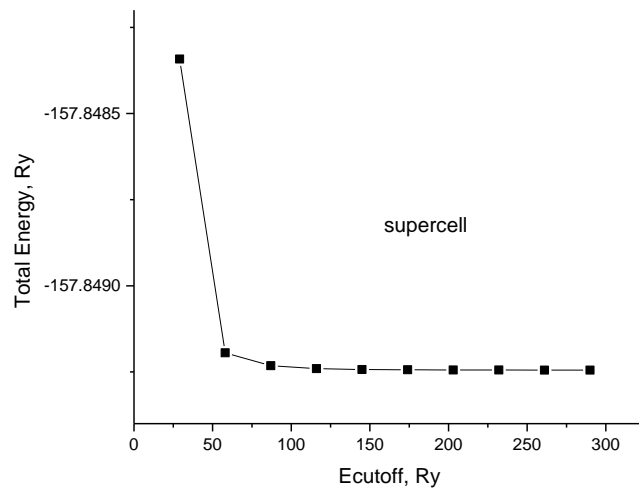


Figure 3.3 Convergence test for bulk Aluminum with respect to energy cutoff

For the calculation of the cohesive energy of Aluminum, a calculation for a spin-polarized isolated atom was carried out. To simulate the condition of the isolated atom, the size of the simulation box should be large enough. A size of 12x12x12 Å was proved to be enough for the calculations. Convergence test with respect to the energy cutoff for the isolated atom was carried out and the result was plotted as shown in **Figure 3.3**. For consistent calculations an energy cutoff of 250 Ry was used.

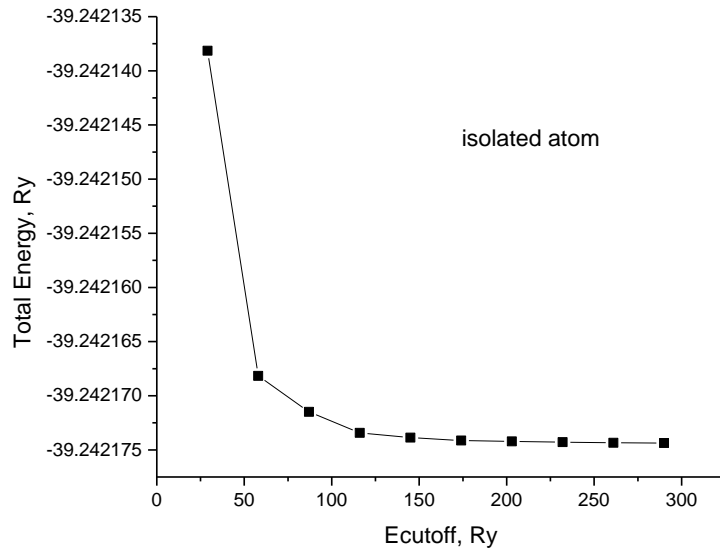


Figure 3.4 Convergence test for isolated Aluminum atom with respect to energy cutoff

To determine the equilibrium lattice parameter and the equilibrium cohesive energy, the cohesive energy for a series of lattice parameters (atomic volumes) calculations were performed.

The cohesive energy is calculated as follows:

$$E_c = \frac{E_{tot}(bulk)}{4} - E_{tot}(isolated)$$

where $E_{tot}(bulk)$ is the total energy of bulk aluminum, and $E_{tot}(isolated)$ is the total energy of isolated aluminum atom.

The minimum of the fitted curve corresponds to the equilibrium values of the lattice parameter and the cohesive energy. From **Figure 3.4**, the equilibrium cohesive energy and the lattice parameters were found to be -3.54 eV/atom and 4.02 Å respectively. These values are in a good agreement with the experimental values, -3.39/-3.39 eV/atom, and 4.05/4.04 Å [63]/ [64].

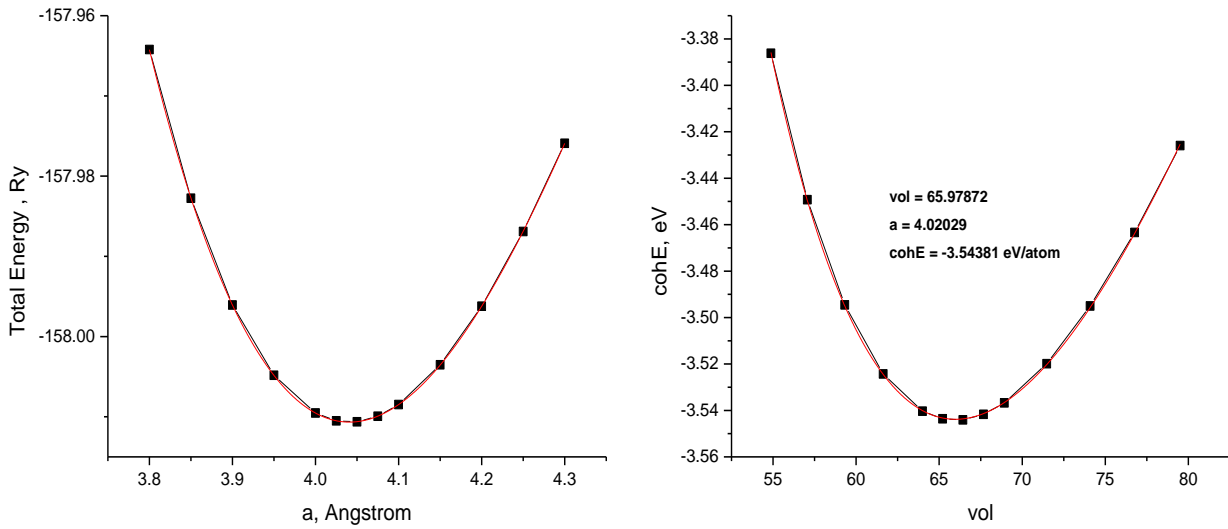


Figure3. 5 The plot of cohesive energy versus series of lattice parameters or unit cell volumes for Aluminum

3.2.2 Copper Bulk properties:

The same computational procedure for aluminum is used for copper except the size of the simulation box for the isolated copper atom was 10x 10x10 Å.

Convergence tests with respect to the size of the k-points grid, shifted and unshifted ones, and to cutoff energy, E_{cut} , and were carried out and the results were plotted as shown in **Figure 3.5**, and **Figure 3.6** respectively. As can be seen from both Figure 3.s, convergence with respect of k-points grid and energy cutoff takes place at values lower than 16x16x16 and 250 Ry respectively;

therefore, these values which are the same ones used for Aluminum are used in the calculations throughout the simulation of Al-Cu alloys and compounds.

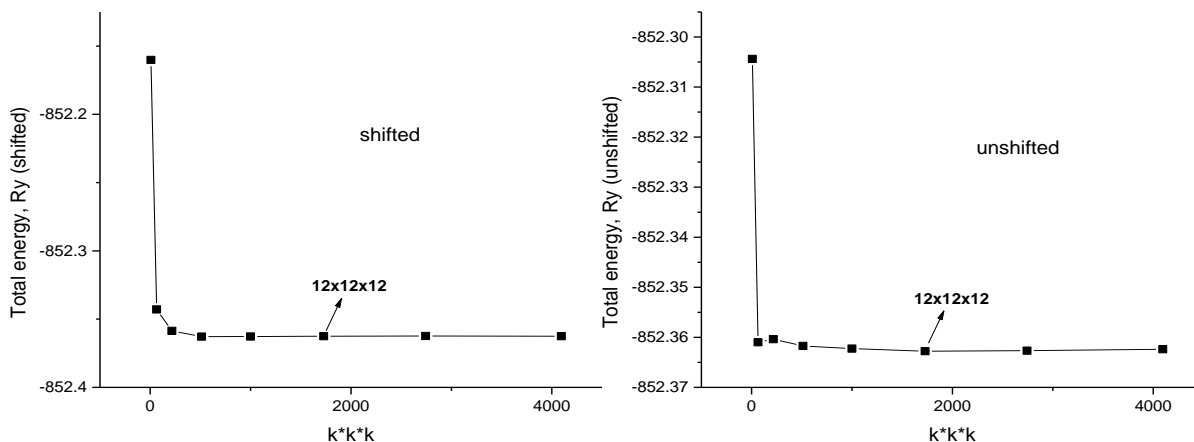


Figure 3.6 Convergence tests for bulk Copper with respect to shifted and unshifted k-points grids

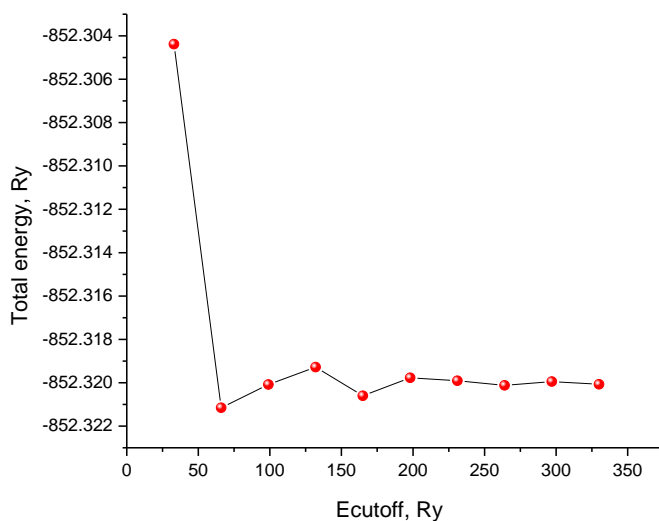


Figure 3.7 Convergence test for bulk Copper with respect to energy cutoff

Convergence test with respect to the energy cutoff for the isolated atom was carried out and the result was plotted as shown in **Figure 3.7**. For consistent calculations an energy cutoff of 250 Ry was used

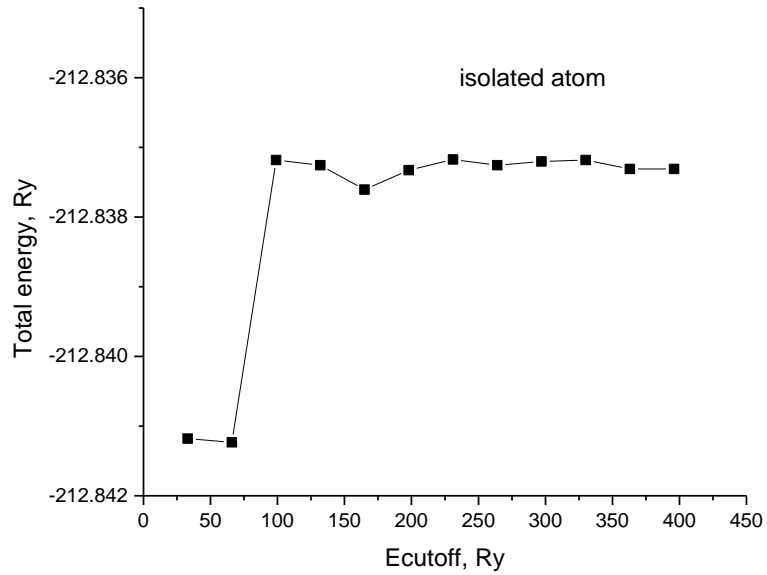


Figure 3.8 Convergence test for isolated Copper atom with respect to energy cutoff

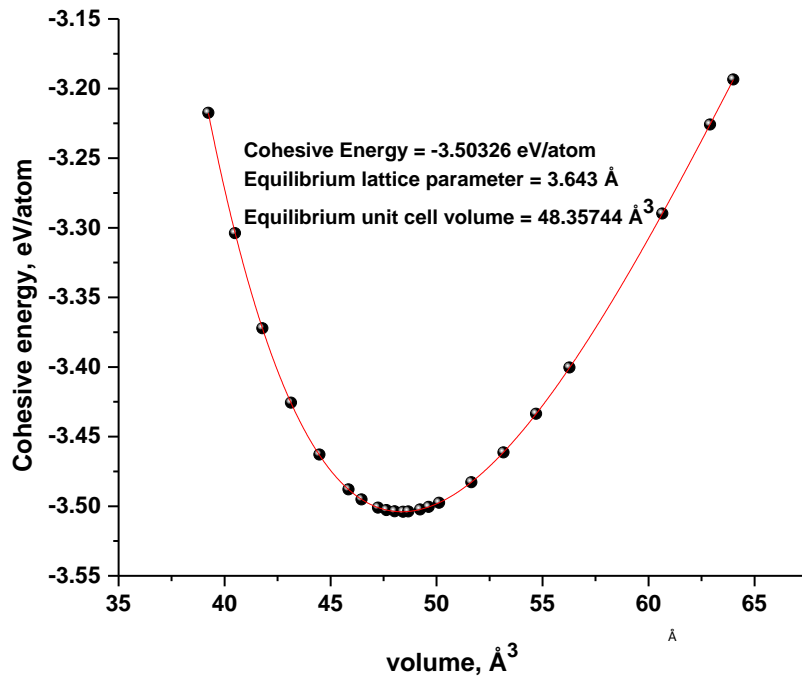


Figure 3.8 The plot of cohesive energy versus series of unit cell volumes for Copper

Equilibrium cohesive energy and lattice parameter for copper were determined from the fitted curve of cohesive energy versus a series of lattice parameters (volumes) as shown in **Figure 3.8**. The equilibrium cohesive energy and the lattice parameters were found to be -3.50 eV and 3.643 Å respectively. These values are in a good agreement with the experimental values, -3.49 eV/atom, and 3.61 Å [14].

3.2.3 Energetics of intermetallics and Al-Cu alloys:

To validate the accuracy of enthalpy of mixing calculations of Al-Cu alloys, the formation and cohesive energies of two intermetallic compounds, namely L1₂ (AlCu₃) and D0₂₂ (AlCu₃), were first calculated. The energy cutoff used in the simulation for both structures were 250 Ry, while the k-points grids of shifted 16x16x16 and shifted 16x16x8 were used for L1₂ (AlCu₃) and D0₂₂ (AlCu₃) structures respectively.

3.2.3.1 The energetics of L1₂ (AlCu₃):

The formation energy of, $\Delta H_f(Al_mCu_n)$, any compound is calculated as follows:

$$\Delta H_f(Al_mCu_n) = \left[E_{tot}^{min}(Al_mCu_n) - \frac{mE_{tot}^{min}(Al)}{4} - \frac{nE_{tot}^{min}(Cu)}{4} \right] / (m + n) \quad (1)$$

$E_{tot}^{min}(Al_mCu_n)$ is the minimum total energy of the intermetallic compound at equilibrium lattice parameter, $E_{tot}^{min}(Al) = -158.01066Ry/4atoms$, $E_{tot}^{min}(Cu) = -852.3789 Ry/4atoms$ are the minimum total energies of the bulk Aluminum and copper at equilibrium lattice parameters.

$E_{tot}^{min}(Al_1Cu_3)(L1_2)$ is determined from the fitted curve of the total energy versus a series of lattice parameters as shown in **Figure 3.9**. $E_{tot}^{min}(Al_1Cu_3)(L1_2) = -678.84055003 Ry/4atoms$.

The formation energy was calculated and found to be

$$\Delta H_f(Al_1Cu_3)(L1_2) - 0.013477 Ry/atom = -0.183 eV/atom$$

This value is in a good agreement with ab initio values, -0.182 eV/atom [54], -0.177 eV/atom [65].

The cohesive energy is calculated as follows:

$$E_c(Al_mCu_n) = [E_{tot}^{min}(Al_mCu_n) - mE_{tot}^{isolated}(Al) - nE_{tot}^{isolated}(Cu)]/(m + n) \quad (2)$$

$$E_{tot}^{isolated}(Al) = -39.24217434 \text{ Ry/atoms} \quad \text{and} \quad E_{tot}^{isolated}(Cu) = -212.83731038 \text{ Ry/atoms}$$

are the total energies of the isolated Al and Copper atoms

The cohesive energy was calculated and found to be

$$E_c(Al_1Cu_3)(L1_2) = -0.2716 \text{ Ry/atom} = -3.694 \text{ eV/atom}$$

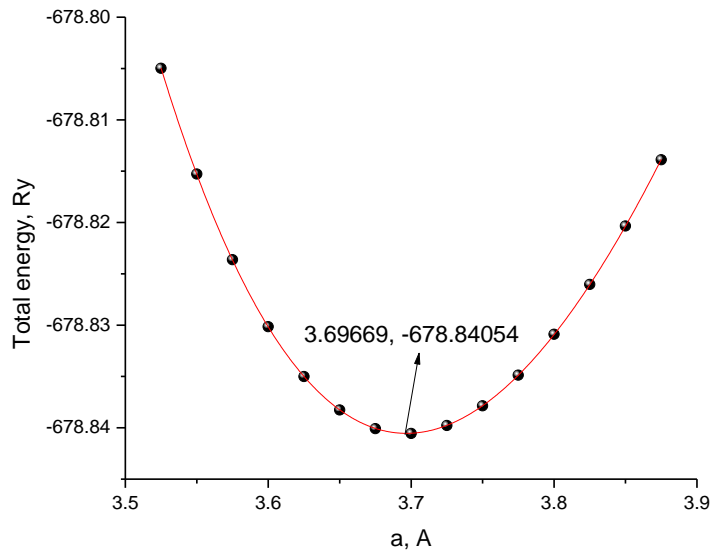


Figure 3. 9 The plot of total energy versus series of unit cell volumes for Copper

3.2.3.2 The energetics of D0₂₂ (AlCu₃):

To calculate the formation and cohesive energies of D0₂₂ (AlCu₃) structure, the total energy of D0₂₂ structure of AlCu₃ was plotted versus series of lattice parameters *a* and the ratio (*c/a*) as a heat map, see Figure 3.10, and splines were used to interpolate between the points, and by

zooming in into it, a and (c/a) were found at the minimum energy, then these values were used to find the minimum total energy of the structure which is used to calculate the cohesive and formation energies and the results are as follows:

$$\mathbf{a = b = 3.674 \text{ \AA}, c = 7.4748 \text{ \AA}}$$

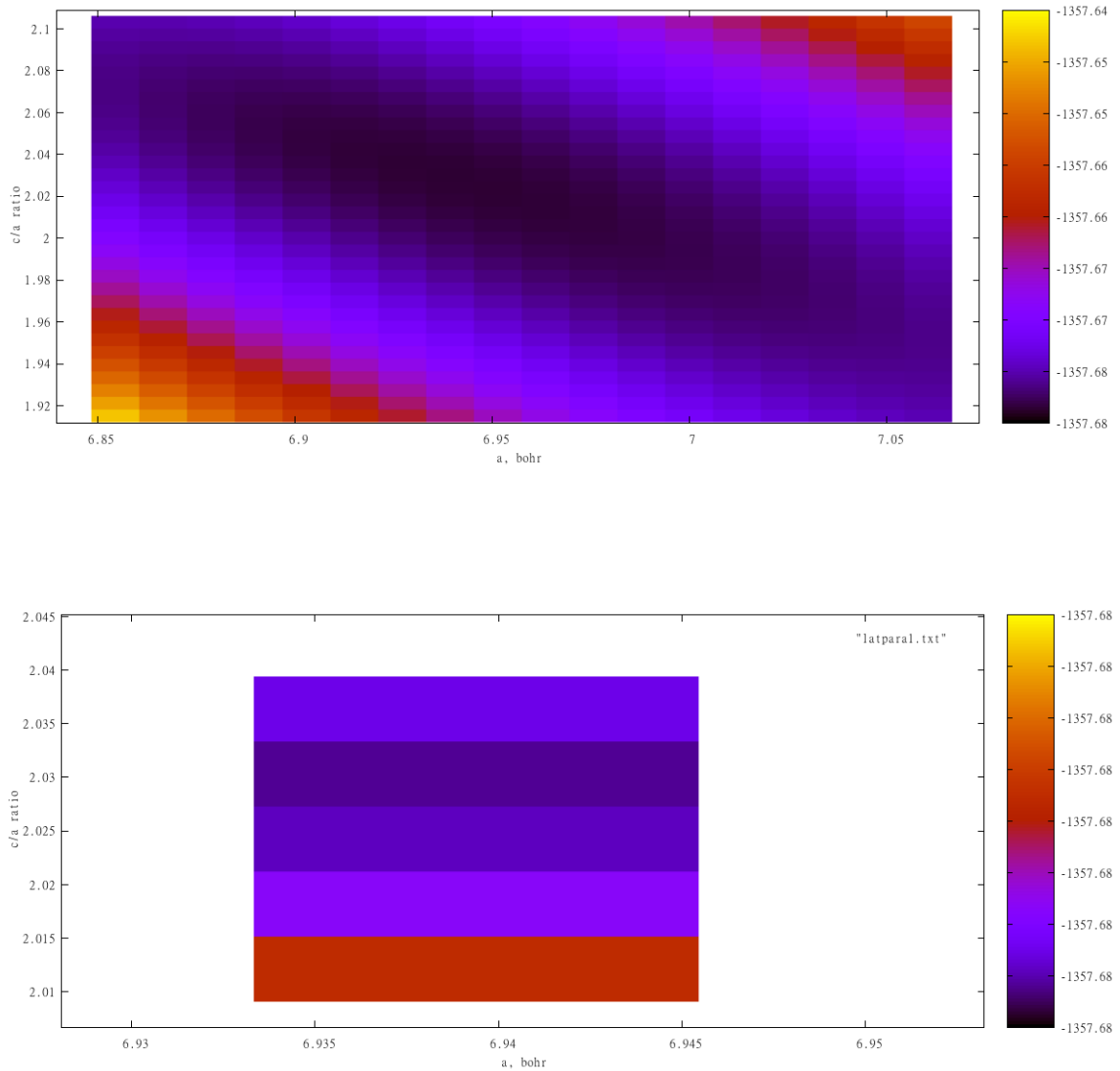


Figure 3.10 The heat map of c/a versus a for $D0_{22}AlCu_3$ structure

$E_{tot}^{min}(Al_2Cu_6)(D0_{22})$ was calculated and found to be = -1357.6853 Ry/8atoms

The formation energy and cohesive energies were calculated using equations (1) and (2) and the results were

$\Delta H_f(Al_2Cu_6)(D0_{22}) = -0.0139525 \text{ Ry/atom} = -0.189754 \text{ eV/atom}$ which is in a good agreement with the ab initio value, -0.185 eV/atom [53].

$E_c(Al_2Cu_6)(D0_{22}) = -0.272 \text{ Ry/atom} = -3.70 \text{ eV/atom}$

3.2.3.3 Energetics of Al-Cu solid solutions:

The mixing enthalpy at T=0 of FCC solid solution was calculated for two different concentrations (**6.25, and 12.5 % Al**) using two different supercells. Both supercells were tetragonal the and the smaller one consisted of two FCC unit cells with one Al atom, while the other one consisted of 4 unit cells with one Al atom. For the smaller supercell a 16x16x8 k-points grid was used while an 8x16x8 was used for the larger supercell. In both supercells Al atom was placed in (0,0,0) position as shown in **Figure 3.11**.

The total energy of each structure of the solid solutions was optimized with respect to the volume, the lattice parameter a and the ratio (c/a) such that the forces on the atoms are very small (less than 2 meV/atom).

The total energy of the small supercell after relaxation was **-1531.22077650 Ry**, and the corresponding mixing enthalpy which is given by equation (2) is **-0.0068795625 Ry/atom** or **-0.09356205 eV/atom**.

The total energy of the larger supercell after relaxation was **-3235.97949062 Ry**, and the corresponding mixing enthalpy is **-0.00349691375 Ry/atom** or **-0.047558027 eV/atom**.

These two results with the results obtained from molecular dynamics simulation, see **Figure 2.11**, confirm that the phases in two-phase region are formed by nucleation and growth and not by spinodal decomposition.

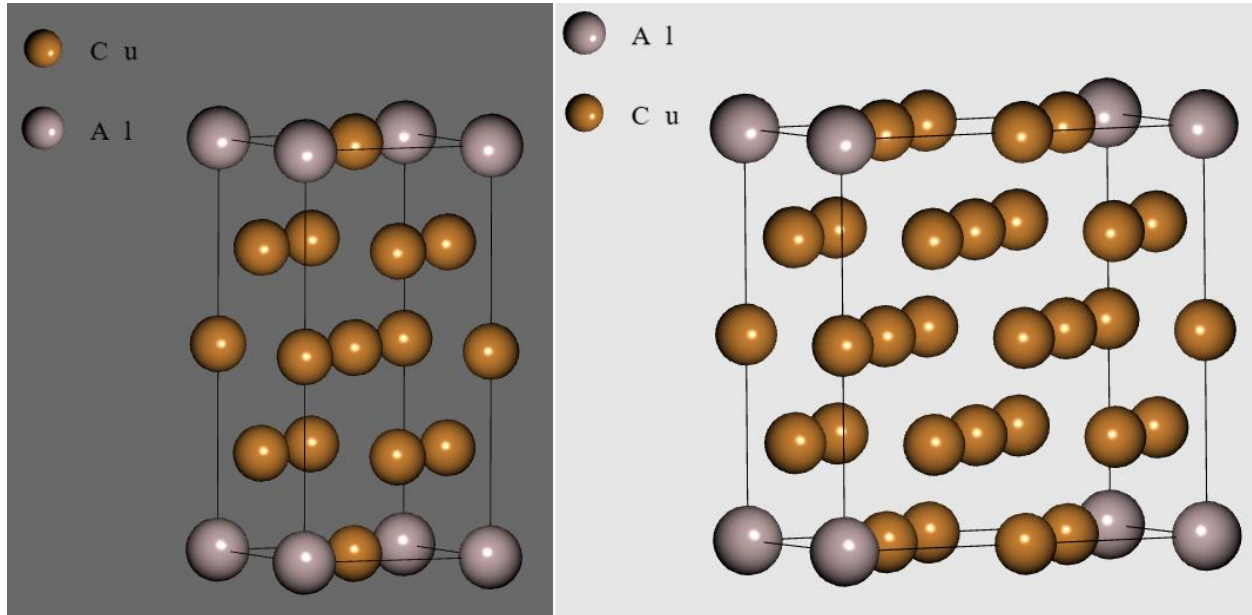


Figure 3.11 The two supercells used in the calculations of mixing enthalpy of 6.25% Al and 12.5% Al solid solutions.

SUMMARY

To address the controversy of whether short-range or long-range ordered domains are obtained upon quenching α phase from above 600°C and subjected to annealing below about 300°C, three computational methods were used, Molecular Dynamics (MD), Hybrid (Monte Carlo) MC/MD, and Density Functional Theory (DFT). Four interatomic potentials were compared with respect to the formation energy to represent Cu-rich side of Al-Cu system. This was achieved by MD, and the EAM potential developed by W. Sheng [49] was chosen to be used throughout hybrid MC/MD simulation.

The MC/MD hybrid method in SGC ensemble was used to study phase separation in the Cu-rich side of Al-Cu system using three starting states, Cu, Al, and Al₄Cu₉ (γ phase), and at three different temperatures, 300, 700, and 1000K. Small and large supercells of these starting states were used. The smaller ones were 500, 500, 520 atoms respectively, and the larger ones were 1372, 1372 and 1404 atoms respectively. These supercells were alloyed in the range of α phase. The plot of equilibrium concentration C_{Cu} (atomic fraction) versus $\Delta\mu$ at each specified temperature for every starting state at the above specified temperatures was plotted and concentration jump was found in all the supercells at 300 and 700K, and this indicates that there is a two-phase region. At 1000 K there was no concentration jump which means that the upper boundary of two-phase region is between 700 and 1000K. Simulation using Cu starting state at 800K was carried out and a concentration jump was obtained in C_{Cu} - versus $\Delta\mu$ plot, and this shifts the upper boundary of two-phase region between 800 and 1000K which is almost the same as for that of the short-range order.

The calculated values of enthalpy of mixing obtained from the MC/MD hybrid simulation that employed smaller supercell Cu starting state at 300K in canonical ensemble were all negative,

hence it can be concluded that the phases in two-phase region are formed by nucleation and growth and not by spinodal decomposition.

The crystal structure within the 2-phase region was visualized using Cu supercell of 25000 atoms (25x25x10) was used. It was found the two-phase region is composed of random α phase and α_2 phase which has a long period superstructure of D0₂₂ and L1₂ [55].

The same 25000 atoms (25x25x10) was used for convergence test and the choice of the Cu supercell with 500 atoms for most of the calculations at 300K was found to be well justified. In DFT simulations (PAW used throughout the simulations [58,49]. To describe the exchange-correlation energy-functional, (GGA) [60] formulated by Perdew, Burke and Ernzerhof (PBE) [61] was used. Methfessel-Paxton [62] smearing of 0.001 Ry was used throughout the simulations. The convergence tests were carried out for Bulk Al and Cu as well as for isolated Al and Cu atoms, and for consistent calculations an energy cutoff of 250 Ry, and a shifted 16x16x16 k-points grid or proper proportions of it were used in all the simulations. The cohesive energies of Al and Cu were calculated and found to be in a good agreement with the experimental values.

To validate the accuracy of enthalpy of mixing calculations of Al-Cu alloys, the formation and cohesive energies of two intermetallic compounds, namely L1₂ (AlCu₃) and D0₂₂ (AlCu₃) were calculated and found to be a good agreement with the ab initio values from literature.

The mixing enthalpy at T=0 of FCC solid solution was calculated for two different concentrations (6.25, and 12.5 % Al) using two different supercells. Both supercells were tetragonal the and the smaller one consisted of two FCC unit cells with one Al atom, while the other one consisted of 4 unit cells with one Al atom. For the smaller supercell a 16x16x8 k-points grid was used while an 8x16x8 was used for the larger supercell. In both supercells Al atom was placed in (0,0,0) position.

The enthalpy of mixing for both concentrations were negative which confirms the results enthalpy of mixing obtained from hybrid MC/MD simulations. This with the other results from hybrid MC/MD simulations confirm that the phases in two-phase region are formed by nucleation and growth and not by spinodal decomposition.

APPENDIX A:

LAMMPS CODES (MOLRCULAR DYNAMICS) used in this work

1- Code to calculate cohesive energy for different structures in Al-Cu system using different interatomic potentials. The structure is defined in another file named "structure.mod" (see for example AlCu3-D022.mod below)

```
include AlCu3-D022.mod
# ----- Define Settings -----
compute eng all pe/atom
compute eatoms all reduce sum c_eng
# ----- Run Minimization -----
reset_timestep 0
fix 1 all box/relax iso 0.0 vmax 0.001
thermo 10
thermo_style custom step temp pe lx ly lz press pxx pyy pzz c_eatoms
min_style cg

minimize 1e-25 1e-25 5000 10000
#-----Calculation of The Concentration of Copper from the Density-----
variable      N equal "count(all)"
variable      teng equal "c_eatoms"
variable      length equal "lx"
variable      ecoh equal "v_teng/v_N"
variable      Volume equal vol
variable      Density equal density
variable      MASS equal "v_Density*v_Volume"
variable      numerator equal "v_MASS*1.0e-24 - 26.982*1.66053904e-24*v_N"
variable      denominator equal "(63.546 - 26.982)*1.66053904e-24*v_N"
variable      Cuconc equal "v_numerator/v_denominator"
```

```

variable      NCu equal "round(v_Cuconc*v_N)"
variable      Accuracy equal "round(v_Cuconc*v_N)-(v_Cuconc*v_N)"
print         "Number of Copper atoms= ${NCu};"
print         "Concentration of Copper = ${Cuconc};"
print         "Accuracy= ${Accuracy};"
print         "Number of all atoms = ${N};"
print         "Lattice constant (Angstroms) = ${length};"
print         "Cohesive energy(eV) = ${ecoh};"
#----SIMULATION DONE-----
print "All done!"

```

```

*****
*****

```

2- File AlCu3-D022.mod used in the previous code

```

*****

```

```

# ----- Initialize Simulation -----
clear
units metal
dimension 3
boundary p p p

atom_style      atomic
atom_modify     map array
#*****AlCu3-D0322 structure*****

variable        latparam equal 5.837
#*****AlCu3-D022***type 1=Al, type2=Cu*****

lattice         custom ${latparam} a1 1.0 0.0 0.0 a2 0.0 1.0 0.0 a3 0.0 0.0 1.0&
                basis 0.25 0.25 0.25 basis 0.75 0.75 0.25 basis 0.75 0.25 0.75 basis 0.25 0.75 0.75&
                basis 0.0 0.0 0.0 &
                basis 0.5 0.0 0.0 basis 0.0 0.5 0.0 basis 0.0 0.0 0.5&
                basis 0.5 0.5 0.0 basis 0.5 0.0 0.5 basis 0.0 0.5 0.5&
                basis 0.5 0.5 0.5&

```

```

basis 0.25 0.25 0.75 basis 0.75 0.75 0.75 basis 0.75 0.25 0.25 basis 0.25 0.75 0.25
region          alcu3box block 0 1.0 0 1.0 0 1.0
create_box      2 alcu3box
create_atoms    1 box &
                basis 1 2 basis 2 2 basis 3 2 basis 4 2

```

```
mass          1 63.546
```

```
mass          2 26.982
```

```
replicate 1 1 1
```

```
# ----- Define Interatomic Potential -----
```

```
#-----EAM potential-----
```

```
pair_style     eam/alloy
```

```
pair_coeff     * * CuAl.eam.alloy Cu Al
```

```
#-----neighbor lists-----
```

```
neighbor 2.0 bin
```

```
neigh_modify delay 10 check yes
```

```
*****
```

3- Example code to use SEMI-GRAND CANONICAL ENSEMBLE to calculate the potential difference versus the concentration of copper

```
*****
```

```
clear
```

```
units          metal
```

```
dimension      3
```

```
package omp    2
```

```
boundary       p p p
```

```
atom_style     atomic
```

```
atom_modify    map array
```

```
#-----
```

```
lattice custom 3.615 a1 1.0 0.0 0.0 a2 0.0 1.0 0.0 a3 0.0 0.0 1.0&
```

```
                basis 0.0 0.0 0.0 basis 0.5 0.5 0.0 basis 0.0 0.5 0.5 basis 0.5 0.0 0.5
```

```
region         AlCubox block 0 5.0 0 5.0 0 5.0
```



```

create_box      2 AlCubox

#-----type 1=Cu, type 2=Al-----
mass          1 63.546
mass          2 26.982
# -----
create_atoms   1 box &
               #basis 1 1 basis 2 1
# -----Interatomic potential-----
pair_style     eam/alloy
pair_coeff     * * CuAl.eam.alloy Cu Al
neighbor      0.50 bin
neigh_modify  every 5 delay 5 check yes
# -----Conjugated gradient minimization-----
min_style     cg
minimize      1e-25 1e-25 10000 10000
#-----TIMESTEP FOR RELAXATION-----
timestep      0.001
#-----
velocity      all create 1300.0 451783253 dist gaussian
#-----
variable      Temperature equal temp
variable      Pressure equal press
variable      N equal "count(all)"
variable      TEnergy equal etotal/v_N
variable      KEnergy equal ke/v_N
variable      Enthalpy equal enthalpy/v_N
variable      PEnergy equal pe/v_N
#-----CalCulation of The Concentration of Copper from the Density-----

```

```

variable      Volume      equal   vol
variable      Density     equal   density
variable      MASS       equal   "v_Density*v_Volume"

variable      numerator   equal   "v_MASS*1.0e-24 - 26.982*1.66053904e-24*v_N"
variable      denominator equal   "(63.546 - 26.982)*1.66053904e-24*v_N"
variable      Cuconc    equal   "v_numerator/v_denominator"
variable      NCu       equal   "round(v_Cuconc*v_N)"
variable      Accuracy  equal   "round(v_Cuconc*v_N)-(v_Cuconc*v_N)"

#-----DATA OUTPUT TO A FILE-----
fix          thermo_out all ave/time 10 1 100 v_Temperature v_Pressure v_TEnergy v_Enthalpy
v_KEnergy v_PEnergy v_NCu v_N v_Cuconc v_Density file
C:/Relaxation//RELAXATION_Cu/DATA_RELAXATION_Cu.out
#-----log file-----

log          C:/lammppwork/RELAXATION_Cu/log.RELAXATION_Cu
#-----RELAXATION (first annealing) -----
fix          9 all npt temp 1300 1000 0.01 iso 0 0 1 pchain 3 mtk yes drag 1
thermo_style custom step temp pe etotal vol enthalpy press density

thermo      1000
run          1000000
unfix       9
#-----RELAXATION (second annealing) -----
fix          10 all npt temp 1000 1000 0.01 iso 0 0 1 pchain 3 mtk yes drag 1

run          4000000
unfix       10
#-----write restart file for relaxation-----

write_restart C:/lammppwork/RELAXATION_Cu/RELAXATION_Cu.rest
#-----alloying with al according to chemical potential difference (SGC ensemble) -----

variable     i equal 0

```

```

variable      iteration equal 5
variable      muAl   equal  0.0
variable      muCu   equal -0.6
variable      a loop  ${iteration}
label         loopa
variable      i equal  ${i}+1
print         "-----"
print         "-----loop number ${i}-----"
print         "-----"
if            "$i==1" then "shell rm data"
variable      delta  equal  0.1
#-----timestep in SGC ensemble-----
timestep 0.0002
#-----

variable      Temperature equal  temp
variable      Pressure    equal  press
variable      N           equal  "count(all)"
variable      TEnergy     equal  etotal/v_N
variable      KEnergy     equal  ke/v_N
variable      Enthalpy    equal  enthalpy/v_N
variable      PEnergy     equal  pe/v_N
#*****Calculation of The Concentration of Copper from the Density*****

variable      Volume      equal  vol
variable      Density     equal  density
variable      MASS        equal  "v_Density*v_Volume"

variable      numerator   equal  "v_MASS*1.0e-24 - 26.982*1.66053904e-24*v_N"
variable      denominator equal  "(63.546 - 26.982)*1.66053904e-24*v_N"
variable      Cuconc      equal  "v_numerator/v_denominator"
variable      NCu         equal  "round(v_Cuconc*v_N)"

```

```

variable      Accuracy      equal  "round(v_Cuconc*v_N)-(v_Cuconc*v_N)"
variableAccuracy equal "round(v_Cuconc*v_N)-(v_Cuconc*v_N)"
#*****

variable      MUAL equal   $\{\mu_{Al}\} + \{\delta\} * (\{i\} - 1)$ 

variable      deltamu equal  $\{\mu_{Cu}\} - \{MUAL\}$ 
log           C:/lammpwork/FCC/Relaxation/NEW/ALCU/ALCU-spinodal-
loop/LOG/log.deltaMu_ $\{\delta\}$ 
#-----

fix           thermo_out all ave/time 10 1 100 v_Temperature v_Pressure v_TEnergy v_Enthalpy
v_KEnergy v_PEnergy v_NCu v_N v_Cuconc v_Density file
C:/lammpwork/SGC/DATA_deltaMu_ $\{\delta\}$ .out
#-----

neighbor      0.50 bin
neigh_modify  every 5 delay 5 check yes

fix          1 all npt temp 1000 1000 0.01 iso 0 0 1 pchain 3 mtk yes drag 1
fix          2 all atom/swap 500 100 9873165 1000 semi-grand yes types 1 2 mu  $\{\mu_{Cu}\}$   $\{MUAL\}$ 

#-----SCREEN OUTPUT-----

thermo_style  custom step temp pe etotal vol enthalpy press density

thermo       1000

#----- visualization-----

dump         1 all xyz 1000 C:/lammpwork/SGC/DUMP/deltaMu_ $\{\delta\}$ .xyz
dump_modify  1 element Cu Al
#-----

run          4000000
#-----

unfix        1
unfix        2
undump       1

#*****Calculation of The Concentration of Copper from the Density*****

```

```

variable      Volume      equal  vol
variable      Density     equal  density
variable      MASS       equal  "v_Density*v_Volume"

variable      numerator   equal  "v_MASS*1.0e-24 - 26.982*1.66053904e-24*v_N"
variable      denominator equal  "(63.546 - 26.982)*1.66053904e-24*v_N"
variable      Cuconcc    equal  "v_numerator/v_denominator"
variable      NCu        equal  "round(v_Cuconcc*v_N)"
variable      Accuracy    equal  "round(v_Cuconcc*v_N)-(v_Cuconcc*v_N)"
print         "Accuracy= ${Accuracy};"
print         "Number of all atoms = ${N};"
print         "Total Energy = ${TEnergy}"
#-----write restart file -----

write_restart C:/lammpwork/SGC/RESTART/deltaMu_${deltamu}.rest
#-----

fix           3 all print 1 " ${MUAL} ${muCu} ${deltamu} ${Cuconcc} " append data
run           1
unfix        3
unfix         thermo_out

#-----to restart from relaxation file for different chemical potential difference-----

include       REST.mod
next          a
jump          AlCu-EAM-spinodal-loop loopa
#*****

4- REST.mod file in the previous code
#*****

clear
units         metal
dimension     3
package omp   2

```

```

boundary      p p p
atom_style    atomic

atom_modify   map array
#-----
read_restart  C:/lampwork /RELAXATION_Cu/RELAXATION_Cu.rest
#-----
pair_style    eam/alloy
pair_coeff    * * CuAl.eam.alloy Cu Al
neighbor      0.50 bin
neigh_modify  every 5 delay 5 check yes
min_style     cg
minimize      1e-25 1e-25 5000 10000

```

5- Example code to use CANONICAL ENSEMBLE to calculate enthalpy and visualize the structure in two-phase region.

```

include      REST_enthalpy.mod
#-----
variable    kassr2 equal 0.06
#-----
set         atom * type/fraction 2 ${kassr2} 719364
#-----
timestep    0.0002
#-----
variable    Temperature equal temp
variable    Pressure equal press
variable    N equal "count(all)"
variable    TEnergy equal etotal/v_N
variable    KEnergy equal ke/v_N

```

```

variable  Enthalpy equal enthalpy/v_N
variable          PEnergy equal pe/v_N
#-----Calculation of The Concentration of Silver from the Density-----
variable  Volume equal vol
variable  Density equal density
variable  MASS equal "v_Density*v_Volume"
variable  numerator equal "v_MASS*1.0e-24 - 26.982*1.66053904e-24*v_N"
variable  denominator equal "(63.546 - 26.982)*1.66053904e-24*v_N"
variable  Cuconc equal "v_numerator/v_denominator"
variable  NCu equal "round(v_Cuconc*v_N)"
variable  Accuracy equal "round(v_Cuconc*v_N)-(v_Cuconc*v_N)"
#-----
log      /home1/04907/khirmas/Visualization_2_phase/log.40000_700K_CONC_${kassr2}_2
#-----
fix      thermo_out all ave/time 100 1 1000 v_Temperature v_Pressure v_TEnergy
v_Enthalpy v_KEnergy v_PEnergy v_NCu v_N v_Cuconc v_Density file
/home1/04907/khirmas/Visualization_2_phase/DATA_40000_700K_CONC_${kassr2}_2.out
#-----
fix      1 all npt temp 700 700 0.01 iso 0 0 1 pchain 3 mtk yes drag 1
fix      2 all atom/swap 100 13333 9873165 700 semi-grand no types 1 2
#-----
thermo_style  custom step temp pe etotal vol enthalpy press density
thermo      1000
dump      1 all xyz 500
/home1/04907/khirmas/Visualization_2_phase/DUMP_40000_700K_CONC_${kassr2}_2.xyz
dump_modify  1 element Cu Al
#-----
run          200000
#-----

```

```

unfix          1
unfix          2
undump        1
#-----Calculation of The Concentration of Copper from the Density-----
print          "Density = ${Density};"
print          "Volume = ${Volume};"
variable MASS equal "v_Density*v_Volume"
variable numerator equal "v_MASS*1.0e-24 - 26.982*1.66053904e-24*v_N"
variable denominator equal "(63.546 - 26.982)*1.66053904e-24*v_N"
variable Cuconc equal "v_numerator/v_denominator"
print          "Concentration of Copper = ${Cuconc};"
variable NCu equal "round(v_Cuconc*v_N)"
print          "Number of Copper atoms= ${NCu};"
variable Accuracy equal "round(v_Cuconc*v_N)-(v_Cuconc*v_N)"
print          "Accuracy= ${Accuracy};"
print          "Number of all atoms = ${N};"
print          "Total Energy = ${TEnergy}"
#-----write restart file-----write_restart
/home1/04907/khirmas/Visualization_2_phase/REST_40000_700K_CONC_${kassr2}_2.rest
#-----
print          "SIMULATION DONE"

```

6- REST_enthalpy.mod file in the previous code

```

clear
units          metal
dimension 3
#package omp    2
boundary  p p p

```



```
atom_style atomic
atom_modify      map array
#-----#-----
read_restart /home1/04907/khirmas/RELAXATION_Cu/RELAXATION_25000_300K_Cu.rest
#read_restart      /home1/04907/khirmas/RESTART/ENTHALPY_25000_CONC_0.06_3.rest
#read_restart /home1/04907/khirmas/Visualization_2_phase/REST_40000_700K__CONC_0.19_1.rest
#-----#-----
pair_style          eam/alloy
pair_coeff          * * CuAl.eam.alloy Cu Al
neighbor           0.50 bin
neigh_modify       every 5 delay 5 check yes
#min_style         cg
#minimize          1e-25 1e-25 5000 10000
```

APPENDIX B:

QUANTUM ESPRESSO CODES (DFT) used in this work:

1- Self-Consistent Field calculation for bulk copper. Same procedure can be followed Aluminum

```
&control
  calculation = "scf"
  restart_mode= "from_scratch"
  pseudo_dir =
"/home1/04907/khirmas/QuantumEspresso/pseudo/Cu/PAW/GGA"
  tprnfor      = .TRUE.
  tstress      = .TRUE.
/
&system
 ibrav = 1
  a =3.643
  nat= 4
  ntyp= 1
  ecutwfc = 250.0
  !ecutrho = 133.0
  occupations ="smearing"
  smearing ="marzari-vanderbilt"
  degauss=0.001
/
&electrons
  diagonalization="cg"
  conv_thr = 1.0e-8
  mixing_beta = 0.7
/
```

ATOMIC_SPECIES

Cu 63.55 Cu.pbe-dn-kjpaw_psl.0.2.UPF

ATOMIC_POSITIONS {crystal}

Cu 0.0 0.0 0.0

Cu 0.5 0.5 0.0

Cu 0.5 0.0 0.5

Cu 0.0 0.5 0.5

K_POINTS (automatic)

16 16 16 1 1 1

2- Self-Consistent Field calculation for isolated copper atom. Same procedure can be followed

Aluminum

&control

calculation = "scf"

restart_mode= "from_scratch"

pseudo_dir = "/home1/04907/khirmas/QuantumEspresso/pseudo"

/

&system

ibrav = 1

a = 10

nat= 1

ntyp= 1

ecutwfc = 250.0

!ecutrho = 133.0

nspin = 2

starting_magnetization(1) = 2.00000e-01

occupations ="smearing"

smearing ="marzari-vanderbilt"

degauss=0.001

```

/
&electrons
  diagonalization="cg"
  conv_thr = 1.0e-8
  mixing_beta = 0.7
/
ATOMIC_SPECIES
Cu 63.55 Cu.pbe-dn-kjpaw_psl.0.2.UPF
ATOMIC_POSITIONS {crystal}
Cu 0.0 0.0 0.0
K_POINTS {gamma}

```

3- Self-Consistent Field calculation for AlCu₃ (D022) structure. Same procedure can be followed for L1₂ structure

```

&control
  calculation = "scf"
  restart_mode= "from_scratch"
  pseudo_dir = "/home1/04907/khirmas/QuantumEspresso/pseudo"

```

```

/
&system
  a = 3.646
  c = 7.533
 ibrav = 6
  nat = 8
  ntyp = 2
  ecutwfc = 250

```

```

!ecutrho = 133.0
occupations ="smearing"
smearing ="marzari-vanderbilt"
degauss=0.001
/
&electrons
  diagonalization="cg"
  conv_thr = 1.0e-8
  mixing_beta = 0.7
/
ATOMIC_SPECIES
Cu 63.55 Cu.pbe-dn-kjpaw_psl.0.2.UPF
Al 26.98 Al.pbe-nl-kjpaw_psl.1.0.0.UPF
ATOMIC_POSITIONS {crystal}
Al   0.000000  0.000000  0.000000
Cu   0.000000  0.500000  0.250000
Cu   0.500000  0.000000  0.250000
Cu   0.500000  0.500000  0.000000
Cu   0.000000  0.000000  0.500000
Cu   0.000000  0.500000  0.750000
Cu   0.500000  0.000000  0.750000
Al   0.500000  0.500000  0.500000
K_POINTS (automatic)
16 16 8 1 1 1

```

4- Varied cell relaxation to relax the 6.25% Al alloy. Same procedure can be followed for 12.5% Al alloy

```

&control

```

```
calculation = "vc-relax"
forc_conv_thr = 1.00000e-03
max_seconds = 8.64000e+04
pseudo_dir = "/home1/04907/khirmas/QuantumEspresso/pseudo"
outdir = "/work/04907/khirmas/stampede2/dump"
tprnfor = .TRUE.
tstress = .TRUE.
/
&system
a = 7.4
b = 3.7
c = 7.4
ibrav = 8
nat = 16
ntyp = 2
ecutwfc = 250
!ecutrho = 133.0
occupations = "smearing"
smearing = "marzari-vanderbilt"
degauss=0.001
/
&electrons
diagonalization="cg"
conv_thr = 1.0e-8
mixing_beta = 0.7
/
&ions
ion_dynamics = "bfgs"
/
```

```

&cell
  cell_dynamics = "bfgs"
  press      = 0.00000e+00
  press_conv_thr = 5.00000e-01
/
K_POINTS {automatic}
8 16 8 1 1 1
ATOMIC_SPECIES
Cu 63.55 Cu.pbe-dn-kjpaw_psl.0.2.UPF
Al 26.98 Al.pbe-nl-kjpaw_psl.1.0.0.UPF
ATOMIC_POSITIONS {crystal}
Al  0.000000  0.000000  0.000000
Cu  0.000000  0.500000  0.250000
Cu  0.250000  0.000000  0.250000
Cu  0.250000  0.500000  0.000000
Cu  0.000000  0.000000  0.500000
Cu  0.000000  0.500000  0.750000
Cu  0.250000  0.000000  0.750000
Cu  0.250000  0.500000  0.500000
Cu  0.500000  0.000000  0.000000
Cu  0.500000  0.500000  0.250000
Cu  0.750000  0.000000  0.250000
Cu  0.750000  0.500000  0.000000
Cu  0.500000  0.000000  0.500000
Cu  0.500000  0.500000  0.750000
Cu  0.750000  0.000000  0.750000
Cu  0.750000  0.500000  0.500000

```

References:

- [1] W. Gaudig and H. Warlimont, *The structure of short range ordered α -Cu-Al alloys and α_2 new superlattice phase*, Acta Metall., 26 (1978) 709.
- [2] S. MURAI, T. HAGA, and S. HIRAYAMA: 1., *Experimental Observation of the Intermediate μ -Phase in Cu-Al β Alloys*, Jpn Inst. Met., 1966,30, 1092-1098
- [3] E. BERNARD and P. DUVAL, *On the period of antiphase domain structures in X- and α_2 -phases of copper-aluminium alloys*, Phys. Status Solidi (a), 1976, 34,135-144.
- [4] N. KUWANO, I. OGATA, Y. TOMOKIYO, and T. EGUCHI, *Formation Process of α_2 Phase in Cu-Al Alloys*, Trans. Jpn Inst. Met., 1977, 18, (3), 195-203.
- [5] N. KUWANO, T. DOI, and T. EGUCHI, *Period of Antiphase and Tetragonality in the α_2 Phase of Cu-Al Alloys*, Trans. Jpn Inst. Met., 1977,18, (11), 807-815.
- [6] J. M. ROLAND, X. QUILLARD, A. MOREAU, and R. GAY, *Analysis of electron diffraction patterns of Cu-Al alloys by Patterson's function*, Phys. Status Solidi (a), 1978, 50, (1), 41-52.
- [7] W. C. Swope, H. C. Andersen, P. H. Berens, and K. R. Wilson, *A computer simulation method for the calculation of equilibrium constants for the formation of physical clusters of molecules: Application to small water clusters*, Journal of Chemical Physics **76**, 637 (1982).
- [8] Rapaport, D.C., *The Art of Molecular Dynamics Simulation*, Cambridge University Press, Cambridge, 1995.
- [9] M. P. Allen and D. J. Tildesley, *Computer Simulation of Liquids* (Clarendon Press, Oxford, 1986).

- [10] N. W. Ashcroft and N. D. Mermin, *Solid State Physics* (Holt, Reinhart & Winston, New York, 1976).
- [11] S. M. Foiles, M. I. Baskes, and M. S. Daw, *Embedded-atom-method functions for the fcc metals Cu, Ag, Au, Ni, Pd, Pt, and their alloys*, *Phys. Rev. B* **33**, 7983 (1986).
- [12] M. S. Daw and M. I. Baskes, *Embedded-atom method: Derivation and application to impurities, surfaces, and other defects in metals*, *Phys. Rev. B* **29**, 6443 (1984).
- [13] M. I. Baskes, J. S. Nelson, and A. F. Wright, *Semiempirical modified embedded-atom potentials for silicon and germanium*, *Phys. Rev. B* **40**, 6085 (1989)
- [14] M. W. Finnis and J. E. Sinclair, *A simple empirical N-body potential for transition metals*, *Phil. Mag. A* **50**, 45 (1984).
- [15] M.S.Daw and M. I.Baskes, *Semiempirical, Quantum Mechanical Calculation of Hydrogen Embrittlement in Metals*, *Phys. Rev. Lett.* **50**, 1285 (1983).
- [16] S. M. Foiles, *Calculation of the surface segregation of Ni-Cu alloys with the use of the embedded-atom method*, *Phys. Rev.* **32**, 7685 (1985).
- [17] F M Marquez et al., *Semigrand-canonical ensemble simulations of the phase diagrams of alloys*, *Modelling Simul. Mater. Sci. Eng.* **11**, 115–126 (2003)
- [18] Alex M. Nieves, V. Vitek, and T. Sinno, *Atomistic analysis of phase segregation patterning in binary thin films using applied mechanical fields*, *Journal of Applied Physics* **107**, 054303 (2010)

- [19] T. Suzudo et al., *Hardening in thermally-aged Fe–Cr binary alloys: Statistical parameters of atomistic configuration*, *Acta Materialia* **89** (2015) 116–122
- [20] Xuyang et al., *Grain Boundary Specific Segregation in Nanocrystalline Fe(Cr)*, *nature, Scientific Reports* **6**, 34642 (2016)
- [21] Vijay Shastry and Diana Farkas, *Modelling Simul. Mater. Sci. Eng.* **4**, 473–492 (1996)
- [22] N. Tajima, O. Takai, Y. Kogure, M. Doyama, *Computer simulation of point defects in fcc metals using EAM potentials*, *Computational Materials Science* **14**, 152-158 (1999).
- [23] Johannes J Möller and Erik Bitzek, *Comparative study of embedded atom potentials for atomistic simulations of fracture in α -iron*, *Modelling Simul. Mater. Sci. Eng.* **22**, 045002 (2014).
- [24] K. O. E. Henriksson, *Molecular dynamics simulations of point defect production in cementite and $Cr_{23}C_6$ inclusions in α -iron: Effects of recoil energy and temperature*, *AIP Advances* **6**, 065010 (2016)
- [25] F Balanchine, J R Kermode, and A De Vita, *Modelling defects in Ni–Al with EAM and DFT calculations* *Modelling Simul. Mater. Sci. Eng.* **24**, 045012 (2016)
- [26] C. A. Becker et al., *Current Opinion in Solid State and Materials Science*, **17**, 277 (2013)
- [27] John R. Smith and Amitava Banerjea, *Origins of the universal binding-energy relation*, *Phys. Rev. B* **37**, 6632 (1988)
- [28] R. A. Johnson, "Alloy models with the embedded-atom" *Phys. Rev. B*, **39**, 12554 (1989).
- [29] Haberlandt, R.; Fritzsche, S.; Peinel, G.; Heinzinger, K.: *Molekularodynamik. Grundlagen und Anwendungen*. Wiesbaden: Vieweg, 1995
- [30] Ercolessi, F.: *A molecular dynamics primer*.

[http://cms.sjtu.edu.cn/doc/reading/md/A_Molecular_Dynamics_Primer_\(Ercolessi\).pdf](http://cms.sjtu.edu.cn/doc/reading/md/A_Molecular_Dynamics_Primer_(Ercolessi).pdf)

[31] Haile, J. M.: *Molecular Dynamics Simulation. Elementary Methods*. New York : John Wiley & Sons, 1997

[32] Chandler, D.: *Introduction to modern statistical mechanics*. New York: Oxford University Press, 1987

[33] Nosé, S.: *A unified formulation of the constant temperature molecular dynamics methods*. *Journal of Chemical Physics*, Vol. 81 (1984), S. 511-519

[34] Hoover, W. G.: *Canonical dynamics: Equilibrium phase-space distributions*. *Physical Review A*, Vol. 31 (1985), S. 1695-1697

[35] Nosé, S.: *A molecular dynamics method for simulations in the canonical ensemble*. *Molecular Physics*, Vol. 52 (1984), S. 255-268

[36] Louwarse, M. J.; Baerends, E. J.: *Calculation of pressure in case of periodic boundary conditions*. *Chemical Physics Letters*, Vol. 421 (2006), S. 138-141

[37] Andersen, H. C.: *Molecular dynamics simulations at constant pressure and/or temperature*. *Journal of Chemical Physics*, Vol. 72 (1980), S. 2384-2393

[38] Hoover, W. G.: *Canonical dynamics: Equilibrium phase-space distributions*. *Physical Review A*, Vol. 31 (1985), S. 1695-1697

[39] Rapaport, D. C.: *The Art of Molecular Dynamics Simulation*. 2, Cambridge: Cambridge University Press, 2004

[40] Parrinello, M.; Rahman, A.: *Crystal Structure and Pair Potentials: A Molecular Dynamics Study*. *Physical Review Letters*, Vol. 45 (1980), S. 1196-1199

- [41] Parrinello, M.; Rahman, A: *Polymorphic transitions in single crystals: A new molecular dynamics method*. *Journal of Applied Physics*, Vol. 52 (1981), S. 7182-7190
- [42] B. Sadigh et al., *Scalable parallel Monte Carlo algorithm for atomistic simulations of precipitation in alloys*, *Physical Review B* **85**, 184203 (2012).
- [43] P. Erhart, A. et al., *Short-range order and precipitation in Fe-rich Fe-Cr alloys: Atomistic off-lattice Monte Carlo simulations*, *Physical Review B* **77**, 134206 (2008).
- [44] P. Giannozzi, et. al., *QUANTUM ESPRESSO: a modular and open-source software project for quantum simulations of materials*, *J.Phys.: Condens. Matter* **21**, 395502 (2009)
- [45] P. Giannozzi, et. al., *Advanced capabilities for materials modelling with Quantum ESPRESSO*, *J.Phys.: Condens.Matter* **29**, 465901 (2017)
- [46] D.M. Ceperley, B.J. Alder, *Ground State of the Electron Gas by a Stochastic Method*, *Phys. Rev. Lett.* **45** (7) (1980) 566.
- [47] J.P. Perdew, et. al., *Atoms, molecules, solids, and surfaces: Applications of the generalized gradient approximation for exchange and correlation*, *Phys. Rev. B* **46** (11) (1992) 6671,
- [48] J.P. Perdew, K. Burke, M. Ernzerhof, *Generalized Gradient Approximation Made Simple*, *Phys. Rev. Lett.* **77** (18) (1996) 3865
- [49] Y. Q. Cheng, E. Ma, and H. W. Sheng, *Atomic Level Structure in Multicomponent Bulk Metallic Glass*, *Phys. Rev. Lett.* **102**, 245501 (2009)
- [50] F. Apostol and Y. Mishin, *Interatomic potential for the Al-Cu system*, *Phys. Rev. B* **83**, 054116 (2011)
- [51] B. Jelinek, S. Groh, M. F. Horstemeyer, J. Houze, S. G. Kim, G. J. Wagner, A. Moitra, and M. I. Baskes *Phys. Rev. B* **85**, 245102 – Published 1 June 2012

- [52] J. Cai and Y.Y. Ye, *Modified embedded atom method potential for Al, Si, Mg, Cu, and Fe alloys*, *Phys. Rev. B* 54, 8398-8410 (1996)
- [35] W. Zhou, L. Liu, B. Li, Q. Song, and P. Wu, *Structural, Elastic, and Electronic Properties of Al-Cu Intermetallics from First-Principles Calculations*, *J. Electron. Mater.* **38**, 356 (2009)
- [54] Alloy database, [<http://alloy.phys.cmu.edu/>] (2005).
- [55] Norbert Ponweiser a, Christian L. Lengauer b, Klaus W. Richter, *Re-investigation of phase equilibria in the system Al–Cu and structural analysis of the high-temperature phase η_1 -Al_{1- δ} Cu*, *Intermetallics* **19** (2011) 1737-1746 and references therein.
- [56] P. Giannozzi, et. al., *QUANTUM ESPRESSO: a modular and open-source software project for quantum simulations of materials*, *J.Phys.: Condens. Matter* **21**, 395502 (2009)
- [57] P. Giannozzi, et. al., *Advanced capabilities for materials modelling with Quantum ESPRESSO*, *J.Phys.: Condens.Matter* **29**, 465901 (2017)
- [58] P.E. Blöchl, *Projector augmented-wave method*, *Phys. Rev.B* 50 (24) (1994) 17953.
- [59] G. Kresse, D. Joubert, *From ultrasoft pseudopotentials to the projector augmented-wave method*, *Phys. Rev. B* 59 (3) (1999) 1758
- [60] J.P. Perdew, J.A. Chevary, S.H. Vosko, K.A. Jackson, M.R. Pederson, D.J. Singh, C. Fiolhais, *Atoms, molecules, solids, and surfaces: Applications of the generalized gradient approximation for exchange and correlation*, *Phys. Rev. B* 46 (11) (1992) 6671
- [61] J.P. Perdew, K. Burke, M. Ernzerhof, *Generalized Gradient Approximation Made Simple*, *Phys. Rev. Lett.* 77 (18) (1996) 3865

[62] M. Methfessel, A.T. Paxton, *High-precision sampling for Brillouin-zone integration in metals*, *Phys. Rev. B* 40 (6) (1989) 3616

Biographical information

Khaled Hirmas Received his B.Sc in Metallurgical and Materials Engineering from the University of Tripoli, Libya in 1992, his first M.S. in Materials Science and Engineering from Christian Albrichts Universität zu Kiel, Germany in 2007, and his second M.S. in Materials Science and Engineering from University of Texas at Arlington where he pursued his Ph.D in Materials Science and Engineering under the supervision of Prof. Choong-Un Kim, and his field of study was the Computational study on the Copper-rich side of Aluminum-Copper Phase Diagram.